REPORT DOCUMENTATION PAGE

AFRL-SR-BL-TR-98-

Public reporting burden for this collection of information is estimated to average 1 hour per response, gathering and maintaining the data needed, and completing and reviewing the collection of information collection of information, including suggestions for reducing this burden, to Washington Headquarter: Davis Highway, Suite 1204, Arlington, VA 22202-4302, and to the Office of Management and Budget, P

ita sources,
oect of this
5 Jefferson

1. AGENCY USE ONLY (Leave blank)	2. REPORT DATE	3.
	16 December 1997	Final Report (1 Aug 94-30 Sept

4. TITLE AND SUBTITLE

Variations in Crust and Upper Mantle Structure Beneath Diverse Geologic Provinces in Asia

5. FUNDING NUMBERS

F4962-94-1-0050

6. AUTHOR(S)

Susan Y. Schwartz

7. PERFORMING ORGANIZATION NAME(S) AND ADDRESS(ES)

University of California, Santa Cruz
Institute of Tectonics/ Earth Sciences Dept.
Santa Cruz, CA 95064

8. PERFORMING ORGANIZATION REPORT NUMBER

9. SPONSORING/MONITORING AGENCY NAME(S) AND ADDRESS(ES)

AFOSR/NM
110 Duncan Avenue, Room B115
Bolling AFB DC 20332-8050
Stanley K. Dickinson/NM

10. SPONSORING/MONITORING AGENCY REPORT NUMBER

11. SUPPLEMENTARY NOTES

12a. DISTRIBUTION/AVAILABILITY STATEMENT

Approval for public release; distribution unlimited

12b. DISTRIBUTION CODE

13. ABSTRACT (Maximum 200 words)

This final report presents results of a two year effort to determine crust and mantle lithospheric structure beneath Eurasia and to explore the effects that structural variations have on regional wave propagation. First, variations in crust and lid structure on Pn and Lg propagation are investigated using regionalized velocity models previously determined under China.. While explosion Pn/Lg ratios are higher than earthquake ratios for all of the regionalized Chinese velocity models, this difference is much smaller than the variations in Pn/Lg ratios caused by propagation differences. This emphasizes the importance of resolving crust and upper mantle structure for successful discrimination. The second part of this report describes detailed regional wave modeling studies to determine crustal and mantle lithospheric structure beneath Tibet. We find low average crustal P-wave velocities (5.9-6.1 km/s), thick crust (68-76 km) and fast lithospheric mantle (8.2-8.25 km/s) beneath the Lhasa Terrane in southern Tibet. Crustal and mantle lithospheric structure to the north in the Qiangtang Terrane differs dramatically with average crustal P- and S-wave velocities 4% faster and 2% slower, respectively relative to the Lhasa Terrane. These differences are too large to be explained by temperature differences alone and require a partially molten uppermost mantle lithosphere in the Qiangtang Terrane.

14. SUBJECT TERMS

Pnl, regional wave propagation, discrimination

15. NUMBER OF PAGES

52

16. PRICE CODE

17. SECURITY CLASSIFICATION OF REPORT	18. SECURITY CLASSIFICATION OF THIS PAGE	19. SECURITY CLASSIFICATION OF ABSTRACT	20. LIMITATION OF ABSTRACT
Unclassified	Unclassified	Unclassified	SAR

NSN 7540-01-280-5500

1998 0129 061

lateral variations in the crust and upper mantle lid structure beneath western China (Beckers et al., 1994). We find a correlation between crust and lid velocity structure and tectonic province. Here we perform a synthetic study to assess how these velocity models affect the propagation of regional phases.

Effects of Variations in Crustal and Upper Mantle Structure on Regional Wave Propagation

The reflectivity technique of Fuchs and Muller (1971) was used to generate synthetic seismograms at regional distances for the four regionalized velocity models we determined beneath China (Beckers et al, 1994, see Figure 1 for models). We used an explosive source located at 500 m depth and an earthquake source at 5 km depth, both with a source duration of 1.5 s. We calculated seismograms at distances of 1° to 10° at 1° increments. The station azimuth for the earthquake source was 22.5°. Due to computational limits we were required to limit the maximum frequency of the synthetic seismograms to 2 Hz. Observed regional waveforms have a frequency content higher than this which limits the extent to which we can quantify the effect of regionalized models on the propagation of the Pn and Lg phases. However, most of the spectral energy of these phases is concentrated below 2 Hz. To effectively generate the Lg phase for the explosion source we included a thin crustal layer at the free surface with a low enough velocity to capture the pS phase in the crust (Frankel, 1989). We used a 3 km thick layer with a P wave velocity of 4.4 km/s. The presence of such low velocities in the uppermost crust is well documented (e.g., Mangino and Ebel, 1992) but in general cannot be resolved by P and PP waveform modeling. The low velocity layer does not have a significant effect on the P and PP waveforms we used in this study because of its limited thickness.

We generated synthetics for the four different models shown in Figure 1. Model WCH was the average model that best fit all our data traversing western China. Models TP, CHE and NCH are appropriate for the Tibetan plateau, eastern and northern China respectively. Pn/Sn velocity ratios in the lid are 1.731 for all models. Synthetic short-period vertical component waveforms for model WCH and an explosive source are shown in Figure 2. The short-period waveforms were generated from broadband displacements through convolution with the response of the Obninsk (OBN) Kirnos

instrument, typical of instruments operating in the former Soviet Union. The synthetics exclude phase velocities smaller than 3.3 km/s to eliminate the high amplitude Rayleigh wave arrivals from the seismograms. The Pn and Lg time windows for computation of root mean square amplitudes (rms) are defined as a constant 10 s window starting just ahead of its onset for Pn, and a phase velocity window between 3.3 and 3.7 km/s for Lg. These windows are indicated on Figure 2.

Figure 3 shows the root mean square amplitude in the Pn and Lg windows for the explosion source and the four different Chinese velocity models. Amplitude differences for the average model WCH and model TP are very small for both Pn and Lg indicating that the higher Pn velocity of the latter model does not change the propagation characteristics of these phases significantly. At distances closer than about 4° the Pn window is contaminated by the inclusion of other phases in the rms window and we therefore comment only on propagation characteristics at greater distances. Between 4° and 10° the increased amplitude of the Pn phase for model CHE relative to the average model WCH can be attributed to the reduced crustal thickness. The effect of the lower P wave velocity in the uppermost mantle for this model is to decrease the Pn amplitude because the increase in ratio between the source P wave velocity and the Pn velocity narrows the range of takeoff angles that will give a critical reflection at the Moho and thus more energy will be lost through radiation into the mantle.

We would expect Pn amplitudes for model NCH to be lower than for model CHE because NCH has both a thicker crust and a lower Pn velocity. However, in contrast we find higher Pn amplitudes increasing with distance. These observations are explained by the positive velocity gradient in the lid for model NCH. The positive lid gradient causes less Pn energy traveling along the bottom side of the Moho to be lost through radiation into the upper mantle. Another effect is that energy that is almost critically reflected at the Moho and penetrates into the lid at near horizontal angles, turns at very shallow depth and can contribute to energy in the Pn window. This latter effect increases with distance accounting for the gain in Pn energy with distance. This increase seems to flatten off near 10° indicating that effect of damping and geometrical spreading are becoming equally important. Though baseline shifts in P velocities in the uppermost mantle do not

influence Pn propagation characteristics very much, variations in lid velocity gradients can significantly change observed Pn amplitudes.

The small difference in Lg energy between models WCH and TP and the significant decrease for models NCH and CHE indicates that, like Pn, crustal thickness is the most important factor controlling Lg energy, with a thicker crust being a better waveguide for this phase. Variations in lid velocities seem to have only a minor effect on the propagation of Lg. Although some scatter is visible, the propagation of Lg seems very stable and the amplitude decay with distance can be well matched by a simple power law equation. The powers of the distance decay rates range between 2.35 and 2.46, intermediate between values for the tectonically active western US. (r^{-3}) and the stable eastern US. (r^{-2}) found by Blanford (1981). Figure 3 demonstrates that differences in propagation for the different models can change Pn/Lg ratios by as much as an order of magnitude. At distances larger than 4°, Pn/Lg ratios increase with distance because the decay of Lg with distance is faster than that of Pn, with the slope of the increase depending on the difference in the decay rate of the two phases.

Figure 4 shows Pn and Lg rms amplitudes for the earthquake source. The behavior of these phases for the four different velocity models is very similar to that of the explosion source with overall amplitudes of both phases reduced by about a decade. To discriminate between earthquakes and explosions we would like the Pn/Lg variations between earthquake and explosion sources to be pronounced and to have a simple predictable behavior. Pn/Lg ratios are often expected to be higher for nuclear explosions than for earthquakes, mainly due to enriched high frequency Pn energy for explosions and enriched Lg for earthquakes. However, the real earth is not that simple. Figure 5 shows the quotient of the explosion and earthquake Pn/Lg ratios. This quotient ranges between 1 and 3 at distances greater than 4°. While explosion Pn/Lg is indeed higher than earthquake Pn/Lg for all of the Chinese velocity models, the difference between the two is smaller than the variations in Pn/Lg ratios caused by propagation differences, which may differ by as much as a factor of 10. Attempts to discriminate between underground nuclear explosions and earthquakes based on Pn/Lg ratios in the passband of our synthetics should therefore be undertaken with great care. This also emphasizes the importance of determining the crust and lid velocity structure in regions where seismic discrimination will be performed.

The next two sections of this report describe modeling of regional phases to determine detailed crustal and lithospheric mantle velocity structures for southern (Lhasa Terrane) and northern (Qiangtang Terrane) Tibet.
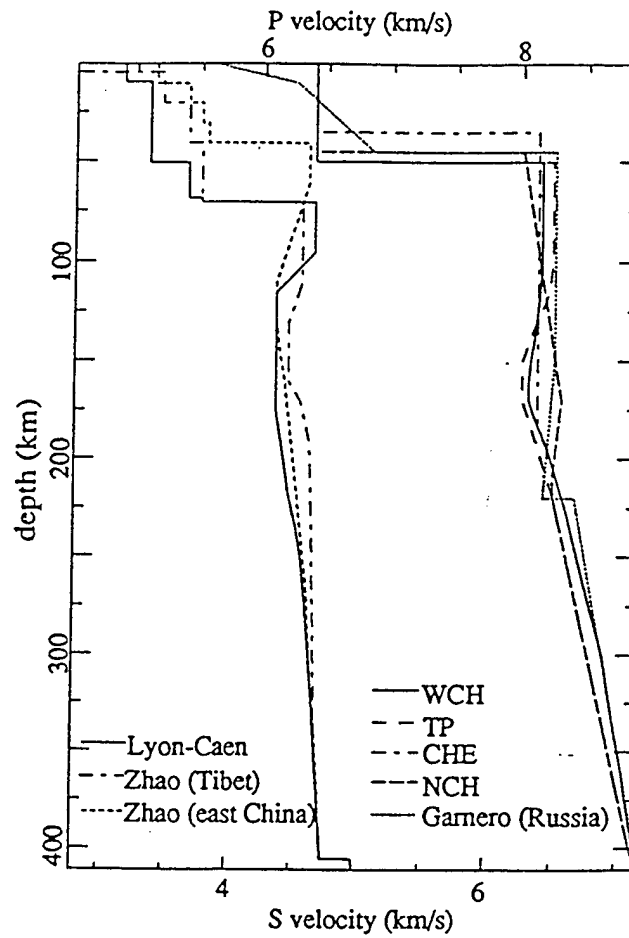
Figure 1 Comparison of the regionalized P wave velocity models derived in this study with and S wave velocity models from previous studies.
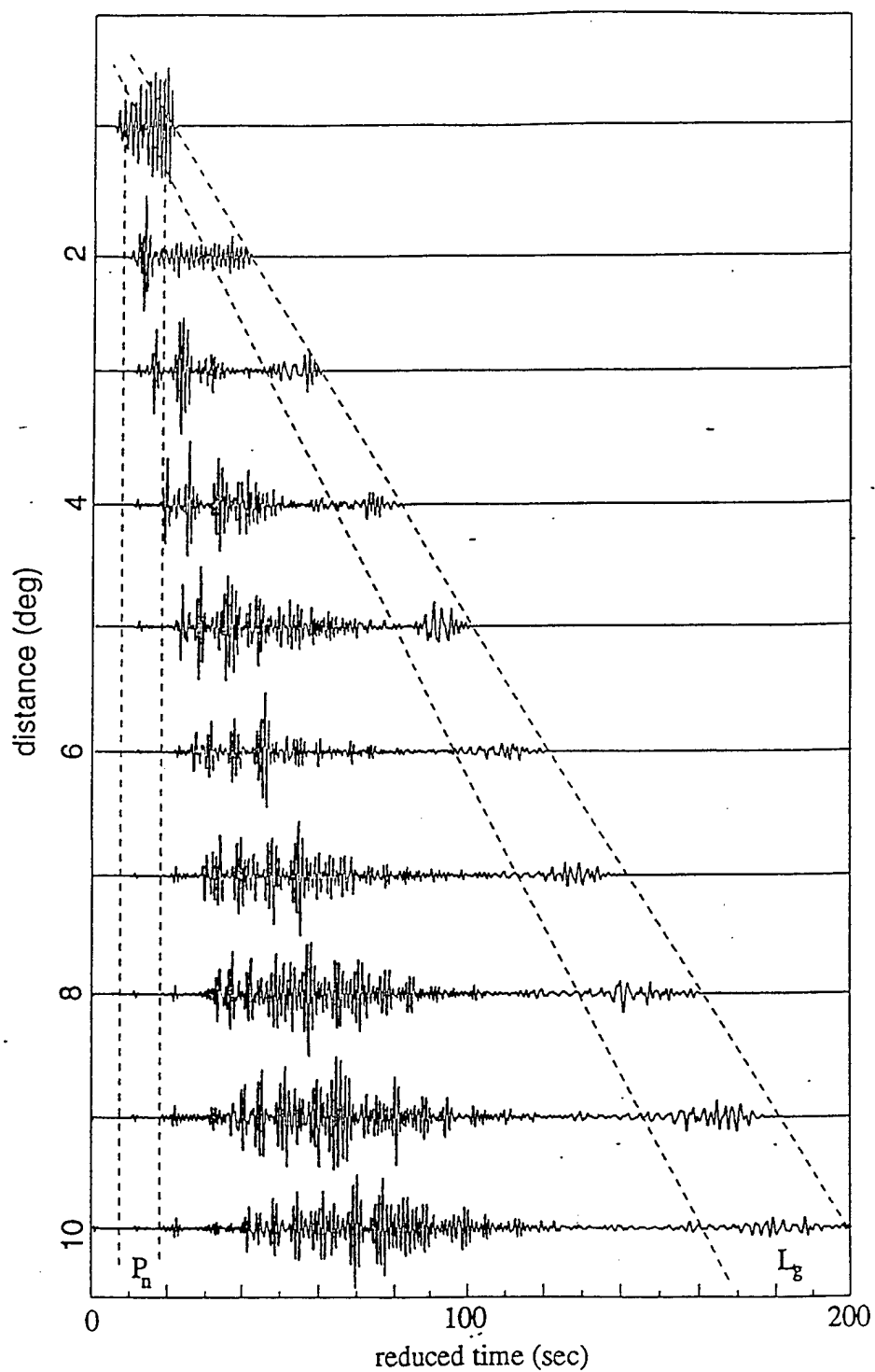
Figure 2. waveforms filtered with the short-period response. Long-period Rayleigh wave modes have dissappeared from the L_g window and the P_n arrival has become more impulsive and complex.
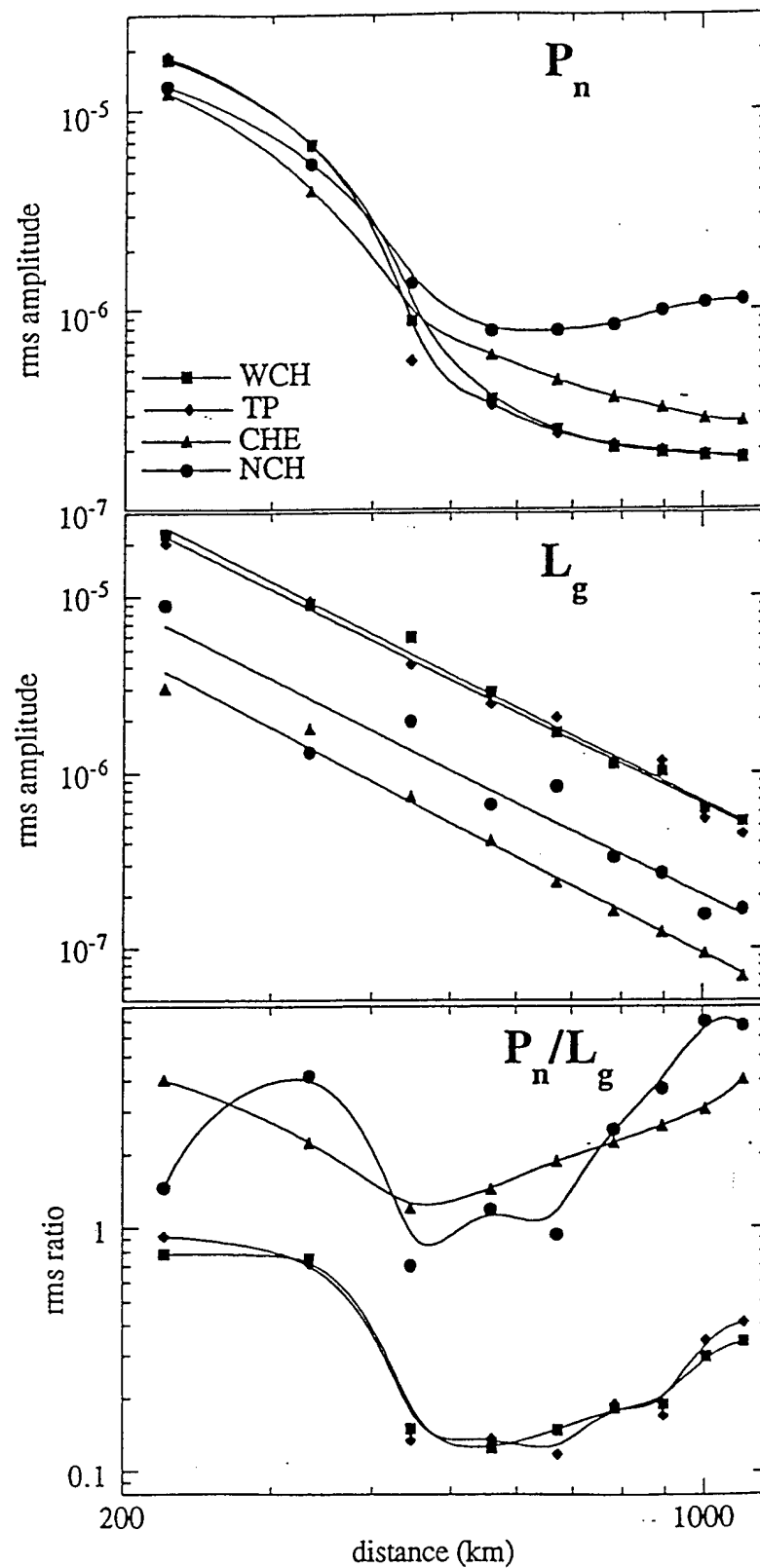
Figure 3 . Short-period rms P_n and L_g amplitudes and their ratios versus distance for 4 different P wave velocity models and the explosive source. The velocity models can be identified in Figure 1
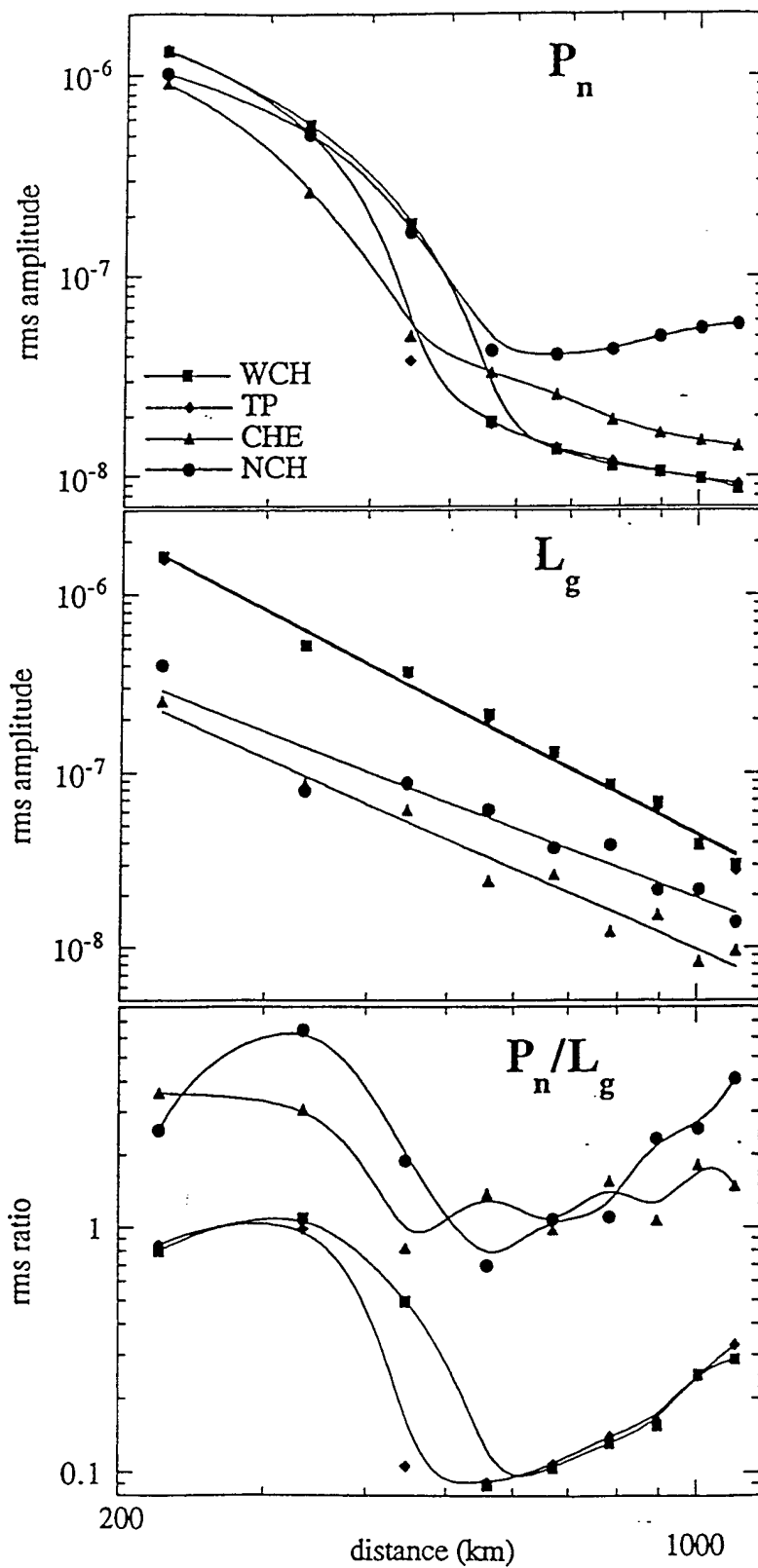
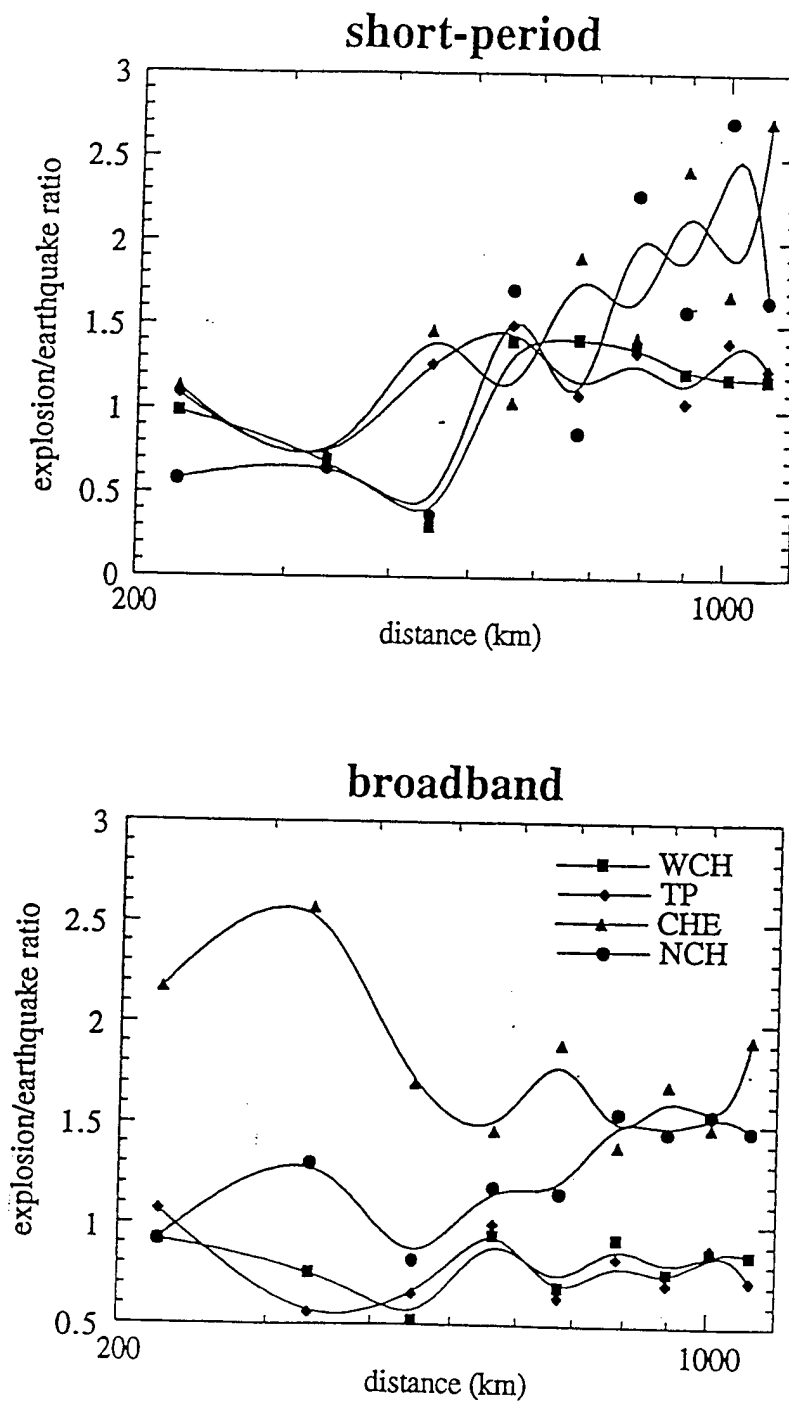*Figure* 4 . Same as Figure 3 but now for the earthquake source.

short-period

broadband

Figure 5 . Quotient of explosion and earthquake P_n/L_g ratios. Though the short-period quotient is consistently higher than 1 for the regionalized Chinese velocity models it is considerably smaller than P_n/L_g variations due to propagation differences

Low crustal velocities and mantle lithospheric variations in southern Tibet from regional Pnl waveforms

Arthur J. Rodgers and Susan Y. Schwartz

Institute of Tectonics and Earth Sciences Department, University of California, Santa Cruz

Abstract. We report low average crustal P-wave velocities (5.9-6.1 km/s, Poisson's ratio 0.23-0.27, thickness 68-76 km) in southern Tibet from modelling regional Pnl waveforms recorded by the 1991-1992 Tibetan Plateau Experiment. We also find that the mantle lithosphere beneath the Indus-Tsangpo Suture and the Lhasa Terrane is shield-like (Pn velocity 8.20-8.25 km/s, lid thickness 80-140 km, positive velocity gradient 0.0015-0.0025 s^{-1}). Analysis of relative Pn travel time residuals requires a decrease in the mantle velocities beneath the northern Lhasa Terrane, the Banggong-Nujiang Suture and the southern Qiangtang Terrane. Tectonic and petrologic considerations suggest that low bulk crustal velocities could result from a thick (50-60 km) felsic upper crust with vertically limited and laterally pervasive partial melt. These results are consistent with underthrusting of Indian Shield lithosphere beneath the Tibetan Plateau to at least the central Lhasa Terrane.

Introduction

The Himalayan Mountains and the Tibetan Plateau resulted from the collision of the Indian and Eurasian Plates. The lithosphere of the Tibetan Plateau was assembled by the accretion of continental and island arc terranes to southern Asia during the closure of the Tethys followed by continental collision (40-50 My ago) and the subsequent northern indentation of the Indian Shield into Asia (e.g., Dewey et al., 1988). Figure 1 shows the major tectonic features of the area. Before the collision of the Indian Shield with Asia convergence was accommodated by oceanic subduction. Paleomagnetic studies indicate that some 2000-3000 km of convergence between the Indian Shield and Eurasia has occurred since the collision although the mechanisms that account for this convergence have been debated (e.g. Dewey et al., 1988; Molnar, 1988; Molnar et al., 1993).

Models of tectonic evolution of the Indo-Eurasian collision can be roughly cast into three end-members: 1) underthrusting of the Indian Shield beneath southern Tibet (Ni and Barazangi, 1983) and/or Asian mantle lithosphere beneath northern Tibet (e.g., Jin et al., 1996); 2) distributed shortening of southern Eurasian crust (e.g., Dewey et al., 1988); 3) injection of Indian crust into Tibetan crust acting to raise Tibet hydraulically (Zhao and Morgan, 1985). Seismic structure of the lithosphere is key to understanding the evolution of this complex region.

Many studies using different data and approaches have inferred seismic structure of the crust and upper mantle beneath Tibet. These studies have reported thick crust (60-75 km), low crustal S-wave velocities, high mantle velocities in southern Tibet and low mantle velocities in northern Tibet (e.g., Molnar 1988; Holt and Wallace, 1990). Deployment of the 1991-1992

IRIS-PASSCAL Tibetan Plateau temporary broadband seismic network provided the first widely available broadband three-component digital seismic waveform data recorded in Tibet (McNamara et al., 1995). In this paper, we report models of the seismic structure of the lithosphere inferred from Pn travel times and Pnl waveforms recorded by the temporary stations.

Data and Methodology

Regional Pnl data are ideal for characterizing the lithosphere because the energy is confined to the crust and the mantle lid. Pnl is a shorthand for the first 60-120 seconds of the long-period P-SV response to crustal excitation and consists of Pn and PL. The first arriving Pn travels in the mantle lid and is sensitive to the P-wave velocities of the lid. PL propagates as a multiply reflected and mode-converted P-SV wave and is sensitive to the average crustal properties. Holt and Wallace (1990; Figure 4) showed that for a given crustal velocity the Pn travel time and Pnl waveform have roughly independent sensitivities to crustal thickness and Pn velocity.

A large (m_b = 6.8) event beneath the Main Central Thrust was recorded by the temporary stations. The event, station and ray paths are shown in Figure 1. Note that the paths are roughly parallel to the main topographic and tectonic features and sample sections of the lithospheric structure perpendicular to the direction of convergence. Instrument deconvolved and bandpass filtered vertical displacement seismograms for this event are shown, along with best-fitting synthetics, in Figure 2. Pn and PL phases are clearly visible and show excellent signal-to-noise and coherence.
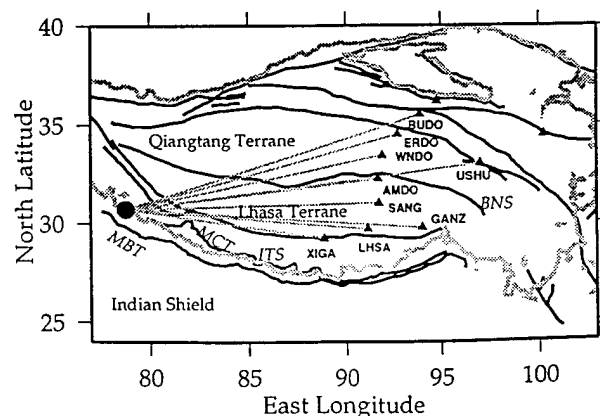

Figure 1. Major tectonic features of the Tibetan Plateau (faults as thick black lines, 3000 m elevation contours as thick grey lines). Tectonic faults are: MBT Main Boundary Thrust; MCT Main Central Thrust; ITS Indus-Tsangpo Suture; BNS Banggong-Nujiang Suture. Locations of the event (circle), stations (triangles) and paths (thin grey lines) are also shown.
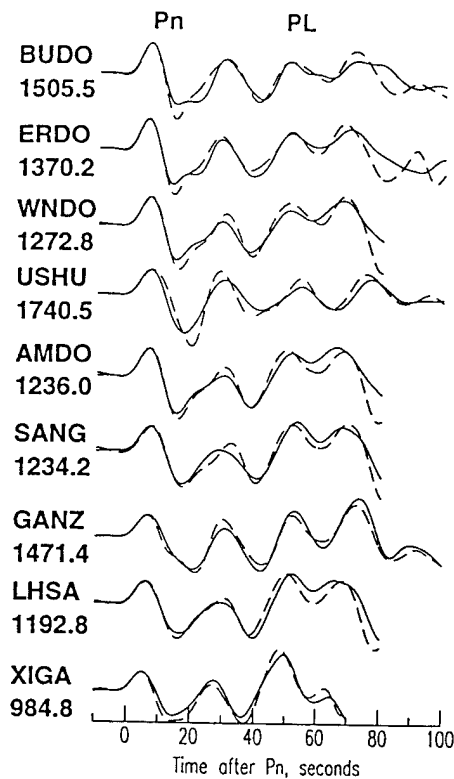
Figure 2. Instrument deconvolved vertical displacement seismograms (solid) and best-fitting synthetics (dashed). Both were passband filtered (0.01-0.1 Hz). Station names and distances are also shown.

We used the ISC location and origin time and the Harvard CMT focal mechanism for this event. Event parameters are: origin time: 1991 Oct. 19 (292) 21:23:15.5, latitude 30.77°, longitude 78.79°, strike 317°, dip 14°, rake 115°. Analysis of this event using local and teleseismic data corroborate these source parameters (Cotton, et al., 1996). The CMT event depth was adjusted from 15 km (below sea-level) to 20 km (below the free surface, at 5 km elevation for the stations used here) by fitting the regional P, pP and sP phases.

Errors in the event location and origin time will map directly into errors in estimates of the absolute velocities, especially mantle velocities. Reasonable estimates of the location error are about 10-20 km (based on ISC, NEIC-PDE and Indian Meteorological Department locations) leading to a 1-2% error in the inferred absolute Pn velocity. Differences in the crustal thickness beneath the event and the path-average will lead to perturbations in the Pn travel times. Analysis of gravity data (Jin et al., 1996) indicates that the crustal thickness beneath the Main Central Thrust is about 40-50 km. certainly less than the 70 km found for the high elevations of the interior of Tibet. We applied an event static correction (1.8 s) to all Pn travel times in order to compensate for possible along-path crustal thickness differences. This correction could be in error by 1.0 s and lead to a 1.0% error in absolute Pn velocity.

Extensive forward modelling efforts were carried out to estimate one-dimensional average velocity structures for each path. Synthetic seismograms for many models of lithospheric structure were computed using the reflectivity method (Fuchs and Muller, 1971). The travel time residual of the first arriving Pn for each model was found by cross-correlating the filtered and scaled Pn waveform with the synthetic. Waveform fit was evaluated by computing the rms difference between the entire Pnl data and the synthetic, shifted to match the Pn arrival time. A small rms difference indicates a good fit. Using an appropriate average lid structure, we concentrated first on determining the average crustal structure by fitting the Pnl waveforms. Then lid parameters were investigated, holding the crustal parameters at their best-fitting values, to fit the Pn arrival time.

Results

Using a mantle structure we found appropriate as an average for all paths (Pn velocity 8.15 km/s, lid thickness 80 km and velocity gradient 0.002 s^{-1}), bulk crustal properties were investigated by computing synthetics for many combinations of crustal thickness and velocities. An upper crustal sediment layer (thickness of 6.0 km; P-wave velocity: 5.0 km/s; S-wave velocity: 2.89 km/s) was used for all models. The long-period data considered here are not strongly sensitive to this layer, however it seems reasonable based on global averages of crustal structure (Christensen and Mooney, 1995). We investigated the fit between data and synthetics for crustal thicknesses of 66-78 km with 2 km increments, crustal P-wave velocities of 5.8-6.3 km/s with 0.1 km/s increments and crustal Poisson's ratios of 0.23-0.29 with 0.02 increments.

Figure 3 shows a contour plot of the rms difference for several paths as a function of the crustal parameters considered.
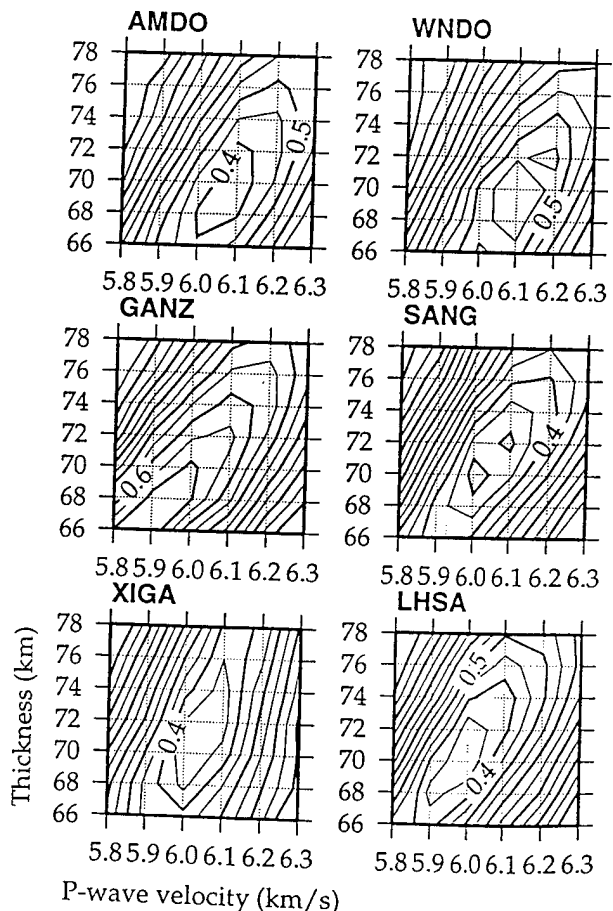

Figure 3. Contours of constant rms difference for the crustal thicknesses and velocities, contour interval 0.05. Crustal Poisson's ratio (0.25) and mantle lid parameters were fixed for each model.

Best-fits are found for a crustal thicknesses of 68-72 km and crustal velocities of 5.9-6.1 km/s. Note that there is a trade-off between these parameters in a direction which preserves the vertical travel time through the crust. The Pnl waveforms are consistently poorly fit for models two grid points away from the best-fitting crustal thickness-velocity pairs. The northern stations prefer slightly higher crustal velocities (AMDO & WNDO 6.0-6.2 km/s) than the southern stations (XIGA, LHSA, GANZ & SANG, 5.9-6.1 km/s). Because the southern paths are contained almost exclusively within the Lhasa Terrane, estimates of crustal structure for these paths are probably better resolved than for the northern paths. McNamara et al. (1995) suggested that the crustal thickness in northern Tibet is 10 km thinner than in the south. Possible along path crustal thickness variations cannot be resolved with the one-dimensional modelling used in this study. The smaller crustal thickness and velocity values for station GANZ may be less reliable because this station is at far regional distance and may be biased by poorly modelled upper mantle triplicated arrivals.

Figure 4 shows the observed and synthetic Pnl waveforms observed at LHSA and SANG for Poisson's ratios, ν, of 0.23, 0.25, 0.27 and 0.29. For each synthetic the crustal thickness and velocity are fixed at 70 km and 6.0 km/s, respectively. The later portion of the PL waveform is sensitive to the crustal Poisson's ratio because P to SV converted energy will arrive later for lower shear-wave velocities (higher Poisson's ratio). Results indicate that a Poisson's ratio of 0.25±0.02 is appropriate for all paths.

Mantle lid parameters were investigated by varying the lid structure while holding the crustal parameters at their best-fitting values. We varied the Pn velocity (8.10-8.25 km/s, 0.05 km/s increment), lid thickness (60-140 km, 20 km increment), and lid gradient (0.001-0.003 s⁻¹, 0.0005 s⁻¹ increment). Figure 5 shows contours of constant Pn travel time residual versus the lid parameters for stations SANG, AMDO and WNDO. Variations in the mantle parameters strongly affect the Pn travel time, while only slightly impacting the waveform misfit.

Figure 5 allows one to find acceptable pairs of lid thickness and gradient for a given Pn velocity. The relative Pn travel time residuals between adjacent paths are insensitive to errors in event location and origin time. Clearly the mantle lid velocities are fast for the path to SANG (Pn velocity 8.20 km/s, lid thickness 80-120 km, lid gradient 0.0015-0.0025 s⁻¹). The fit to the other southern stations (XIGA, LHSA & GANZ) require slightly faster mantle lid parameters. The travel times require an abrupt decrease in the average mantle lid velocities beneath the northern Lhasa Terrane, the Banggong-Nujiang Suture (BNS) or the southern Qiangtang Terrane. The paths to the more northern stations (ERDO & BUDO, not shown) require further reductions in the average mantle lid velocities.
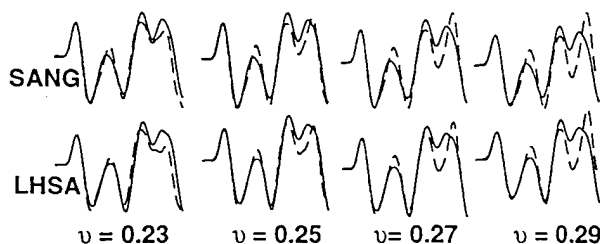

Figure 4. Observed (solid) and synthetic (dashed) waveforms for Poisson's ratios (ν = 0.23-0.29). Crustal thickness and P-wave velocity were fixed to 70 km and 6.0 km/s.
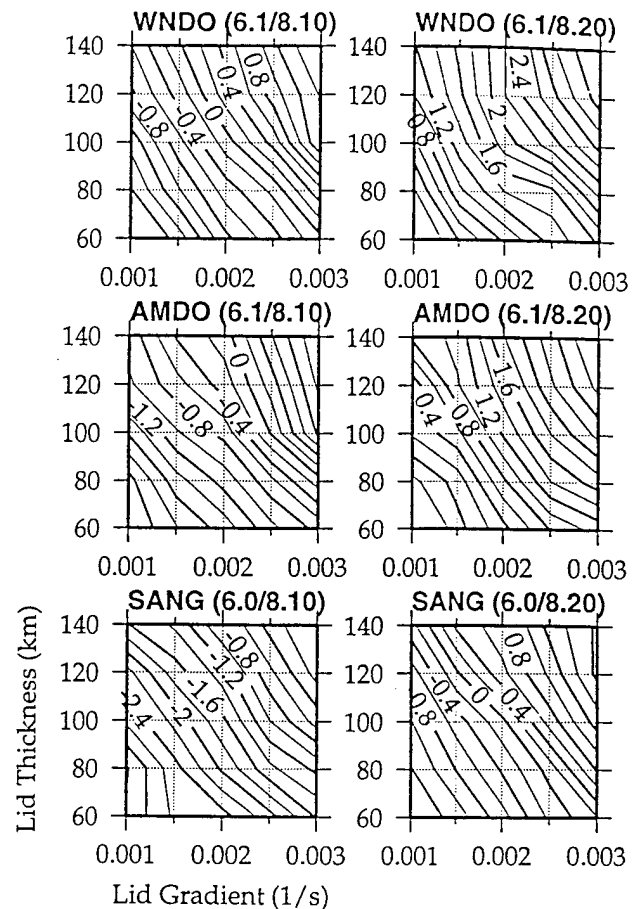

Figure 5. Contours of constant Pn travel time for various lid thicknesses and gradients, contour interval 0.2 seconds. Crustal parameters were fixed at their best-fitting values. The crustal and Pn velocities are given in parenthesis above each panel.

Discussion and Conclusions

An estimate of the global average crustal velocity was reported by Christensen and Mooney (1995) to be 6.45 ± 0.23 km/s. Average crustal velocities are slightly lower for orogenic belts: Christensen and Mooney (1995) reported 6.39 ± 0.25 km/s; Zandt and Ammon (1995) reported 6.25 ± 0.25 km/s. The average crustal velocities we found for southern Tibet (5.9-6.1 km/s) are 1-2 standard deviations below the averages given above. Recently, low average crustal velocities (6.0 km/s) were reported for the Altiplano of South America (Zandt et al., 1996). This high plateau results from crustal thickening due to oceanic subduction of the Nazca Plate beneath the western South American Plate. Zandt et al. (1996) suggested that the velocities result from a predominantly felsic composition. Compilations of laboratory measurements of seismic velocities at crustal temperatures and pressures indicate that such low average velocities are only possible for felsic compositions in high heat flow conditions (Christensen and Mooney, 1995).

The Altiplano observation is relevant to Tibet because, although the current tectonics are quite different, it is well established that before continental collision oceanic subduction was occurring on the southern margin of Asia forming the Gandese batholith directly north of the Indus-Tsangpo Suture and thickening the southern Lhasa Terrane (Dewey et al., 1988). Low velocities in the crustal sections associated with this former

back-arc could be due to the presence of a predominately felsic crust. It is now well established that the Indian Shield is underthrusting southern Tibet (e.g Jin et al., 1996). If the Indian Shield is typical of other Precambrian shields it is composed of a felsic upper crust (2/3, including sediments) overlying a mafic lower crust (1/3). Underthrusting of some of the Indian crust beneath the Tethyan Himalayas and felsic Lhasa Terrane would create a 50-60 km thick felsic upper crust. Assuming a high heat flow (e.g. 90 mW/m^2), temperatures of about 800-1000° C would be reached in the depth range 30-50 km. Depending on the amount of water present at depth, such a thick felsic crust could undergo partial melting. Although the solidus of dry granitic compositions is in excess of 1200° C, even relatively small amounts of water (0.7 wt%) can lower the solidus to near 700° C (Huang and Wyllie, 1981). Therefore the plausible presence of a small amount of water would generate some melt in these compositions at depth. Furthermore, felsic compositions have higher heat productions (Rudnick and Fountain, 1995), which would also act to raise crustal temperatures, enhance melt and lower seismic velocities. Extensive partial melt in the crust would raise Poisson's ratio (>0.3) and probably result in wide spread volcanism. Because neither of these are observed for southern Tibet, a thick (≥ 35 km), laterally pervasive layer of partially melted crust seems unlikely. The crustal velocity profiles inferred by Zhao et al. (1996) do not support or refute a thick laterally pervasive melted layer.

Although we cannot determine layered crustal structure, the petrological considerations above suggest that melt in the crust is likely. A recent study by Kind et al. (1996) reported evidence for a mid-crustal S-wave low velocity zone (20 km thick, consistent with partial melt) overlying a higher velocity layer for a short inter-station line (130 km) in southern Tibet, north of the ITS, but not south of the ITS. Such a low velocity mid-crustal layer may be associated with a laterally pervasive weak zone that mechanically decouples the upper crust from the lower crust as suggested by Zhao and Morgan (1985) and Jin et al. (1996) or simply an isolated zone of partially melted crust. Our bulk crustal properties are consistent with Kind et al.'s (1996) model (average S-wave velocity of 3.40-3.46 km/s). Because our results provide constraints for long (≈ 1000 km) regional paths, mostly north of the ITS, it is possible that melt in a thin (≈ 20 km) layer is laterally pervasive in the crust of southern Tibet.

The Pn travel time data considered here reveal fast shield-like mantle velocities beneath the southern and central Lhasa Terrane and an abrupt decrease in the mantle velocities beneath the northern Lhasa Terrane and BNS. The high inferred Pn velocities imply that temperatures are relatively low directly beneath the Moho. Results from short-period Pn tomography (McNamara et al., 1996) indicate that resolvable differences in the Pn velocity exist beneath the Lhasa and Qiangtang Terranes (approximately 8.20-8.30 km/s and 8.00-8.10 km/s, respectively). The long-period waveform data considered here, which are sensitive to deeper mantle lid structure, show that a thick mantle lid with a positive velocity gradient is associated with the tomographically inferred fast Pn velocities beneath the Lhasa Terrane. Taken together, the inferred crustal and mantle structure suggest that the crust and the mantle lithosphere of the Indian Shield are underthrusting the Tethyan Himalayas and Lhasa Terrane and that Indian mantle lithosphere has penetrated at least to the central Lhasa Terrane, possibly to the Banggong-Nujiang Suture.

References

Christensen, N. and Mooney, W. Seismic velocity structure and composition of the continental crust: A global view, *J. Geophys. Res.*, *100*, 9761-9788, 1995.

Cotton, F., Campillo, M., Deschamps, A. and Rastogi, B., Rupture history and seismotectonics of the 1991 Uttarkashi, Himalaya earthquake *Tectonophysics*, *258*, 35-51, 1996.

Dewey, J., Shackleton, R., Chengfa, C. and Yiyin, S., Tectonic evolution of the Tibetan Plateau, *Philos. Trans. R. Soc. of London, Ser. A*, *327*, 379-413, 1988.

Fuchs, K. and Muller, G., *Computation of synthetic seismograms with the reflectivity method and comparison with observations, Geophys. J. Royal Astro. Soc. 23*, 417-433, 1971.

Holt, W. and Wallace, T. Crustal thickness and upper mantle velocities in the Tibetan Plateau region from the inversion of regional Pnl waveforms: Evidence for a thick upper mantle lid beneath southern Tibet, *J. Geophys. Res.*, *95*, 12,499-12,525, 1990.

Huang, W., and Wyllie, P., Phase relationships of S-type granite with H$_2$O to 35 kbar: muscovite granite from Harney Peak, South Dakota, *J. Geophys. Res.*, *86*, 10,515-10,529, 1981.

Jin, Y., McNutt, M., and Zhu, Y. Mapping the descent of the Indian and Eurasian plates beneath the Tibetan Plateau from gravity anomalies, *J. Geophys. Res.*, *101*, 11,275-11,290, 1996.

McNamara, D., Owens, T. and Walter, W. Observations of regional phase propagation across the Tibetan Plateau, *J. Geophys. Res.*, *100*, 22,215-22,229, 1995.

McNamara, D., Walter, W., Owens, T. and Ammon, C. Upper mantle structure beneath the Tibetan Plateau from Pn travel time tomography, in press *J. Geophys. Res.*, 1996.

Molnar, P. A review of geophysical constraints on the deep structure of the Tibetan Plateau, the Himalaya, and the Karakoram and their tectonic implications, *Phil. Trans. R. Soc. Lond.*, *A326*, 33-88, 1988.

Molnar, P., England, P., and Martinod, J., Mantle dynamics, uplift of the Tibetan Plateau, and the Indian Monsoon, *Rev. geophys. 31*, 357-396, 1993.

Kind, R., 9 others, Mid-crustal low velocity zone beneath the southern Lhasa Block: results from the INDEPTH-II earthquake recording program, in press *Science*, 1996.

Rudnick, R., and Fountain, D., Nature and composition of the continental crust: a lower crustal perspective, *Rev. Geophys.*, *33*, 267-309.

Zandt, G. and Ammon, C., Continental crust composition constrained by measurements of crustal Poisson's ratio, *Nature*, *374*, 152-154, 1995.

Zandt, G., and 7 others, Anomalous crust of the Bolivian Altiplano, central Andes: Constraints from broadband regional seismic waveforms, *Geophys. Res. Lett.*, *23*, 1159-1162, 1996.

Zhao, L.-S., Sen, M., Stoffa, P. and Frolich, F., Application of very fast simulated annealing to the determination of the crustal structure beneath Tibet, *Geophys. J. Int.*, *125*, 355-370, 1996.

Zhao, W., and Morgan, W., Uplift of the Tibetan Plateau, *Tectonics, 4*, 359-369, 1985.

A. J. Rodgers and S. Y. Schwartz, Earth Sciences Department, University of California, 1156 High Street, Santa Cruz, CA 95064.

Lithospheric Structure of the Qiangtang Terrane, Northern Tibetan Plateau from Regional Complete Waveform Modelling: Evidence for Partial Melt

Arthur J. Rodgers

Earth Sciences Division, Lawrence Livermore National Laboratory, Livermore, CA, USA

Susan Y. Schwartz

Institute of Tectonics and Earth Sciences Department, University of California, Santa Cruz, CA, USA

Abstract

We report models of P- and S-wave velocity and attenuation for the the crust and mantle lithosphere of the Qiangtang Terrane, northern Tibetan Plateau inferred by fitting reflectivity synthetic seismograms to the observed regional waveforms. The data used are three-component broadband seismograms recorded by the 1991-1992 IRIS-PASSCAL Tibetan Plateau Experiment and Global Seismic Network (IRIS-GSN) stations in the region. The Qiangtang Terrane has thick crust (65 ± 5 km) with P- and S-wave velocities of 6.1-6.3 and 3.34-3.43 km/s, respectively, yielding an anomalously high crustal Poisson's ratio of 0.29 ± 0.02. Seismic velocities of the mantle lithosphere of the Qiangtang Terrane are normal for P-waves and slow for S-waves (8.0-8.1 and 4.35-4.40 km/s, respectively) yielding a high mantle Poisson's ratio of 0.29 ± 0.01. Attenuation in the crust and mantle lid is high (Q_P = 100-200 and Q_S = 44-89). Modelling of the broadband P-waveforms suggests that the mantle lid may be at least 75 km thick, however this is not unambiguously supported by the data. The crust and mantle lithosphere of the Qiangtang Terrane probably contains partial melt based on the high Poisson's ratio, low shear wave velocities and low Q. The absence of high-frequency Sn and the presence of volcanism of mantle lithospheric origin support the presence of partial melt.

Crustal and mantle lithospheric structure in the Qiangtang Terrane is different from that for the Lhasa Terrane (immediately to the south), based on results of previous studies. The average crustal P- and S-wave velocities are 4% faster and 2% slower, respectively, in the Qiangtang Terrane relative to the Lhasa Terrane. This yields a significant difference in the crustal Poisson's ratio with values of 0.29 for the Qiangtang Terrane and 0.25 for the Lhasa Terrane. Differences in the mantle P- and S-wave velocities and Poisson's ratios of these two adjacent terranes cannot be explained by temperature differences alone. Our results are consistent with McNamara et al., 1997 (approximately a 300°C temperature difference in the mantle) and a partially molten uppermost mantle lithosphere in the Qiangtang Terrane.

Introduction

The Tibetan Plateau is the largest region of elevated topography and thickened continental crust on Earth and is widely considered as the type-example of continental collision. A complex history of Tethyan oceanic subduction, terrane accretion and continental collision of the Indian and Eurasian Plates has lead to the current configuration of the plateau (Figure 1; Allegre et al., 1984; Searle et al., 1987; Dewey et al., 1988). Competing and sometimes mutually exclusive mechanisms have been proposed for the evolution of crustal thickening of the Tibetan Plateau (e.g., Powell and Conaghan, 1973; Barazangi and Ni, 1982; Ni and Barazangi, 1983; Allegre et al., 1984; Zhao and Morgan, 1987; Dewey et al., 1988; Molnar, 1988; Molnar et al., 1993; Fielding et al., 1994). Although these studies have used diverse geologic and geophysical evidence, seismic structure of the lithosphere provides important constraints on the large-scale spatial and long-term temporal evolution of the Indo-Eurasian collision. Because of the importance of continental collision in the formation of the continents, understanding the structure and dynamics of this region informs our understanding of continental evolution in general.

Previous studies of seismic structure of the Tibetan Plateau reported thick crust ($\approx$ 70 km), low crustal P- and S-wave velocities and significant differences in mantle lithospheric structure between the southern and northern Tibetan Plateau (e.g., Patton, 1980; Chen and Molnar, 1981; Romanowicz, 1982; Hirn et al., 1984; Sapin, et al., 1985; Jobert et al., 1985; Brandon and Romanowicz, 1986; Chun and McEvilly, 1986; Molnar, 1988; Bourjot and Romanowicz, 1992; Molnar et al., 1993; McNamara et al., 1995, 1997; Herquel et al., 1995; Rodgers and Schwartz, 1997), In particular, fast shield-like mantle velocities were reported for southern Tibetan Plateau while slower mantle velocities and the absence of short-period regional S-waves were reported for north-central Tibetan Plateau (e.g., Chen and Molnar, 1981, Ni and Barazangi, 1983; Brandon and Romanowicz, 1986; Lyon-Caen, 1986; Holt and Wallace, 1990; Beghoul et al., 1993; Zhao and Xie, 1993; McNamara et al., 1995; Wittlinger, et al., 1996; Rodgers and Schwartz, 1997; McNamara et al., 1997).

The 1991-1992 IRIS-PASSCAL Tibetan Plateau Experiment recorded broadband seismic data on a north-south line across the Tibetan Plateau (Owens et al., 1993; McNamara et al., 1994, 1995, 1996, 1997). This experiment provided the first widely available digital seismic data recorded across the plateau. The station distribution (Figure 1) allows resolution of structural variations within the plateau itself, which was difficult if not impossible with previous data sets. Analysis of these data have resulted in a tremendous advancement of knowledge of the large-scale lithospheric structure of the Tibetan Plateau. Several studies used these data to infer crustal structure by modelling broadband teleseismic body-waves (Zhu et al., 1993; Zhu et al., 1995; Zhao et al., 1996). These studies all agree that the crust is thick

(55-80 km) although they disagree on some of the details of the structure. Recently, Owens and Zandt (1997) modelled shear-coupled teleseismic P-waves to infer crustal structure across the Tibetan Plateau and found large variation in crustal thickness (75 km in the Lhasa Terrane to 55 km in the Songpan-Ganzi Terrane) and Poisson's ratio (0.27 in the Lhasa Terrane to 0.33 in the Songpan-Ganzi Terrane). The previously reported first-order differences between mantle structure of the southern and northern Tibetan Plateau have been confirmed and more clearly defined by the IRIS-PASSCAL data. McNamara et al. (1995) reported that a zone of inefficient Sn propagation (indicated by the absence of short-period regional Sn and originally reported by Ni and Barazangi, 1983) is larger and is correlated with the tectonic province boundaries of the Qiangtang (Chang Tang) Terrane and the (northern) adjacent Songpan-Ganzi Terrane. Recent volcanism of mantle lithospheric origin in the northern Tibetan Plateau over-lies the region of inefficient Sn propagation (Turner et al., 1993, 1996). No such recent vol-canism has been observed in the southern Tibetan Plateau. A Pn tomography study by McNamara et al. (1997) found that shallow mantle P-wave velocities are 8.1-8.3 km/s beneath the Lhasa Terrane but are reduced to 7.9-8.1 km/s beneath the Qiangtang and Songpan-Ganzi Terranes. The boundary between these zones of differing mantle structures approximately lies at the Banggong-Nujiang suture (BNS, Figure 1). Using the IRIS-PASSCAL data, Rodgers and Schwartz (1997) found that shield-like thick, positive velocity gradient mantle lithosphere underlies the Lhasa Terrane, and that mantle P-wave velocities decrease abruptly across the BNS. Thus, the higher resolution results from analysis of the 1991-2 IRIS-PASSCAL data set provides substantial evidence for significant lateral thermal and/or compositional variations between the southern and northern Tibetan Plateau. These extreme differences in the mantle structure exist despite the remarkable absence of topographic relief and Bouguer gravity anomalies across the plateau (e.g., Fielding et al., 1994; Jin et al., 1994).

Of particular interest to this study is the structure of the mantle lithosphere and its impli-cations for dynamical models of Tibetan Plateau evolution. In the southern Tibetan Plateau observations of fast, shield-like mantle beneath the Lhasa Terrane has been cited as evidence for dynamical models of underthrusting of cold Indian Shield continental lithosphere (Ni and Barazangi, 1983; Holt and Wallace, 1990; Rodgers and Schwartz, 1997). High velocities have been inferred to depths of 250-400 km in the upper mantle beneath the Himalaya and Karakoram and have been cited as evidence for downwelling of continental mantle (Molnar, 1990; Molnar et al., 1993; Pandey et al., 1995; Woodward and Molnar, 1995; Zhou et al., 1996). The occurrence of earthquakes in the mantle lithosphere (depths of 70-113 km; e.g., Zhu and Helmberger, 1996a) beneath the High Himalaya suggests that temperatures there are in the range 500°-700° C (Ruppel and McNamara, 1997). However, observations of slower mantle P-wave velocities along with the absence of high-frequency Sn beneath the Qiangtang

and Songpan-Ganzi Terranes (McNamara et al., 1997; McNamara et al., 1995) and volcanic evidence (Turner et al., 1993, 1996) imply higher temperatures and possibly partial melt in the shallow mantle. Brandon and Romanowicz (1986) reported low sub-Moho S-wave velocities (4.4-4.5 km/s) in the Qiangtang Terrane and suggested the possibility that the mantle lithospheric lid is absent. Such seismic observations have been used to support models of mantle lithospheric delamination (e.g., Bird, 1978) and convective instability (Molnar et al., 1993). These models state that either asthenospheric mantle has infiltrated a void left by the negatively buoyant cold mantle lithosphere (delamination) or that downwelling of thickened mantle lithosphere beneath the southern Tibetan Plateau is accompanied by upwelling of asthenospheric mantle beneath the northern Tibetan Plateau (convective instability). Both of these models could site the observed low mantle seismic velocities as evidence of asthenospheric temperatures. A lower bound for asthenospheric temperatures is about 1250°C, the dry peridotite solidus. However, extremely large (north-south) lateral temperature differences of 550°-750°C would result from such scenarios, given the intermediate depth earthquakes in the southern Tibetan Plateau. Interpretation of the observed Pn velocities when the effect of attenuation is properly accounted for does not require asthenospheric temperatures in the mantle at shallow depths (McNamara et al., 1997). More realistic temperature differences between the northern and southern Tibetan Plateau are 240°-370°. The composition and physical properties of the lithosphere of the northern Tibetan Plateau are key to discriminating between the proposed models of Tibetan Plateau evolution.

In this paper, we report models of lithospheric structure of the northern Qiangtang Terrane of the Tibetan Plateau inferred by modelling broadband seismic waveforms from regional earthquakes. The observed waveforms reveal great sensitivity to lithospheric structure. The inferred seismic velocity and attenuation structure provides constraints on the composition and thermal structure of the Tibetan Plateau. Results reveal low crustal and mantle S-wave velocities and high Poisson's ratio and suggest that partial melt is present in the crust and shallow mantle. Differences in the seismic velocity structure of the Qiangtang and Lhasa Terranes will be quantified and interpreted by comparing the results of this study to our previous results for the southern Tibetan Plateau (Rodgers and Schwartz, 1996, 1997).

Data and Methodology

Whereas early seismic studies of Tibetan Plateau structure relied heavily on data recorded at stations adjacent to the plateau, more recent data with paths entirely within the Tibetan Plateau lithosphere are less likely to be impacted by lateral variations in structure associated with the plateau's boundaries (especially crustal thickness variations). For such data the modelling assumption of a one-dimensional velocity structure is more appropriate.

Figure 1 shows the events and stations used in this study. We made use of three events recorded by the 1991-2 IRIS-PASSCAL Tibetan Plateau experiment (1992/096 and two events on 1992/179 in the northern Tibetan Plateau). Permanent broadband stations operated by the Global Seismic Network (IRIS-GSN) in the region also recorded some of these events. Supplementary constrains on the focal depth, mechanism and velocity structures were obtained from data recorded at the permanent stations. The excellent pure-path sampling of the Qiangtang Terrane provided by these data was exploited to infer average one-dimensional velocity structures from these data.

Regional seismic data are most sensitive to the structure of the lithosphere (the crust and mantle lithosphere or mantle lid). Complete seismograms consist of the body and surface waves (Pn, PL, Sn, Love and Rayleigh). For distances less than about 1600 km the observed complete regional waveforms are less sensitive to structure below the seismic low velocity zone. As seismic energy hits the low-velocity zone, it is refracted away from the lithosphere and reaches the surface at far-regional distances (greater than 1600 km). At distances greater than about 1600 km large amplitude energy is reflected and refracted by upper mantle discontinuities at 410 and 660 km depth and this results in triplicated body-wave arrivals. For short paths contained within a single tectonic province, lithospheric structure can be well approximated by a one-dimensional model and excellent fits to the observed regional waveforms can be obtained. The important features of such structures are crustal thickness, average crustal P- and S-wave velocities (V_P and V_S, respectively) and attenuation, sub-Moho P- and S-wave velocities, velocity gradients and attenuation and the thickness of the mantle lid. The arrival times of body-wave phase such as Pn and Sn are mainly sensitive to the uppermost mantle P- and S-wave velocities, respectively. The waveform shape of the long-period shear-coupled P-wave, PL, is mostly sensitive to the vertical P-wave travel time in the crust (V_P times crustal thickness), however this phase has some sensitivity to the shear velocities in the crust (e.g., Helmberger, 1972; Shaw and Orcutt, 1984; Wallace, 1986; Holt and Wallace, 1990; Rodgers and Schwartz, 1997). The Pn and PL phases are often referred to jointly as Pnl. The Love and Rayleigh (surface) waves are sensitive to the crustal thickness and the shear velocity structure of the crust and upper most mantle. Love waves have no sensitivity to P-wave velocity structure and Rayleigh waves are only weakly sensitive to shallow P-wave velocity structure. The simultaneous determination of P- and S-wave velocities allows us to estimate Poisson's ratio, which is helpful for inferring composition. Recent reviews of laboratory measurements of the physical properties of crustal and upper mantle compositions provide the necessary links between inferred seismic velocity and petrologic structures (Christensen and Mooney, 1995; Rudnick and Fountain, 1995; Christensen, 1996).

Reliable modelling of complete seismograms requires accurate knowledge of the earth-quake focal depth and mechanism and the source-time function must be simple enough to be represented by a displacement step-function at the periods modelled. Events with complicated moment release will not be well modelled by synthetic seismograms, particularly at higher frequencies. We began this analysis by considering only events for which Harvard Centroid Moment Tensors (CMT, Dziewonski et al., 1983) were available. Generally, these are events which have body-wave magnitude, m_b, greater than or equal to 5.5 as reported by the National Earthquake Information Center-Preliminary Determination of Epicenters (NEIC-PDE). Such events often have excellent signal-to-noise at regional distances. Smaller events with source parameters from other bulletins were also used (discussed below). Only double couple components of the moment tensor were used when computing synthetic seismograms. Focal depths and mechanisms for the three events modelled were evaluated by comparing the observed waveforms for regional data to reflectivity synthetics and observed teleseismic P-waves were compared to WKBJ synthetic seismograms using the source parameters (Table 1). All events required evaluation and possibly revision of the reported Harvard CMT or NEIC-PDE focal depths. Event epicenters were taken from the NEIC-PDE. Table 1 lists the source parameters of the earthquakes studied.

Observed waveforms were compared to reflectivity synthetic seismograms (Fuchs and Muller, 1971). Many lithospheric velocity structures were investigated using a grid-search technique. An earth flattening approximation was applied to all velocity models. A grid search technique applied to waveform modelling is computationally intensive as it requires the calculation of many synthetic seismograms, but the resulting synthetics reveal the sensitivity of the data to each model parameter investigated. Furthermore, grid search allows for a wide range of models to be considered. This is superior to inversion schemes that are highly sensitive to a starting model. The models we investigated were initially made to be as simple as possible to first constrain average crustal and mantle lid elastic structure by accurately predicting the timing and amplitudes of the main phases. More complex elastic and anelastic structures were investigated once an appropriate average elastic structure was estimated. For all models a sediment layer was assumed (4 km thickness, P- and S-wave velocities of 5.0 and 2.89 km/s, respectively). Investigations of various sediment layer structures found that the data are not highly sensitive to this layer for the frequencies considered. Nonetheless, it seems appropriate to include such a layer given the pervasive presence of sediment layers in reported models of average crustal structure (Christensen and Mooney, 1995; Rudnick and Fountain, 1995). Given the appropriate focal mechanism and depth, synthetics for each event-station pair were computed for each velocity structure. Following the procedure first outlined by Rodgers and Schwartz (1997), we determined the travel time residual of the

filtered and scaled first arrival (usually Pn), then evaluated the waveform misfit by computing the rms difference and linear correlation between data and delayed synthetic. Generally, we compared the data and synthetics in the pass band 10-100 seconds (0.01-0.1 Hz). For periods shorter than 10 seconds complex crustal layering and possible lateral structure probably makes the assumption of a one-dimensional model less appropriate. For periods longer than about 50 seconds the sensitivity to detailed lithospheric structure is greatly diminished.

Results - The 1992/096 Event and Development of the Qiangtang Terrane Model

Excellent pure-path sampling of the Qiangtang Terrane was obtained by the 1991-2 IRIS-PASSCAL deployment for a regional event in the northwestern Tibetan Plateau (Figure 1). The paths to stations AMDO, WNDO, ERDO and USHU are exclusively confined to the Qiangtang Terrane. This event was large enough (m_b = 5.6) to be observed teleseismically and a focal mechanism was found by the Harvard CMT project (depth 17 km, strike 62°, dip 52° rake -11°). A focal mechanism was also determined by Zhu and Helmberger (1996b) using regional waveform data (depth 10 km, strike 210°, dip 50° rake -90°). Figure 2a shows the broadband regional Pn and pPn waveforms observed at several stations and synthetic seismograms for these focal mechanisms. The depth was fixed at 10 km and synthetics were computed using our Qiangtang Terrane model (see below). The Harvard CMT mechanism for this event predicts near-nodal dilatational first motions to stations AMDO, ERDO and LHSA, while compression is observed. The Harvard CMT focal mechanism is determined by model-ling long-period body and surface waveforms, mostly at teleseismic distances. We found that changes in the strike and rake away from the Harvard CMT mechanism resulted in misfit of the surface waveforms. Adjustments of the dip (from 52° to 90°) using a grid search technique resulted in improved fits to the observed Pn and pPn waveforms to the temporary stations and permanent IRIS-GSN stations WMQ, AAK and GAR. Note that the Pn and pPn pulses at station WMQ are best represented by our mechanism.

The focal depth can be inferred by fitting the broadband Pn and (surface reflected) pPn phases. Figure 2b shows the Pn and pPn waveforms observed at station AMDO for depths of 5, 10, 15 and 20 km. For these investigations we used the Qiangtang Terrane model described below. Clearly, a depth of 10 km provides the best fit to the Pn-pPn timing. Teleseismic P-waves for this event were obtained for three IRIS-GSN stations. Figure 2c shows the fit of WKBJ synthetic seismograms computed with the three focal mechanisms to the observed P-waves with the depth fixed at 10 km. The stations used are: KIV (distance 30.1°, azimuth 293°) KONO (distance 50.6°, azimuth 322°) and MDJ (distance 37.9°, azimuth 61°). These data are somewhat noisy, but our adjustment to the depth and dip of the Harvard

CMT mechanism seems appropriate as it improves the fit to the observed waveforms at all stations. Investigation of the focal depth with these teleseismic data supported our estimate of the depth (10 km). Although details of the broadband waveforms after the pPn arrival in Figures 2a and 2b are not well fit, the improved focal parameters (depth 10 km, strike 62°, dip 90°, rake -11°) provide the best fit to the relative timing and amplitude of Pn and pPn at most stations. Conservative uncertainties in these focal parameters are less than 5 km in depth and 20° in fault plane orientation based on the misfit to the observed data seen in grid search results. Slightly smaller errors were reported by Randall et al. (1995) using regional long-period complete waveforms.

The best-fitting lithospheric velocity structures were inferred by numerous synthetic seismogram computations. These investigations resulted in the Qiangtang Terrane model (Table 2). The analysis proceeded by first estimating the average crustal thickness, P-wave velocity and Poisson's ratio by fitting the Pnl and complete waveforms. The mantle S-wave velocity and Poisson's ratio were estimated by fitting the Sn-Pn travel time. Mantle lid structure was found by fitting the broadband P-waveforms. Finally the resulting model was verified by considering the fits to the complete three-component waveforms and to other paths confined to the Qiangtang Terrane for two other events.

Pnl Waveforms, Crustal Thickness, P-wave Velocity and Poisson's Ratio

Pnl waveforms recorded at the IRIS-PASSCAL stations were used to infer average pure-path crustal thickness and velocity structure for the Qiangtang Terrane. Similar to the grid search analysis applied by Rodgers and Schwartz (1997), we investigated: crustal thicknesses of 55-70 km, 5 km increment; crustal P-wave velocities of 5.9-6.4 km/s, 0.1 km/s increment; and crustal Poisson's ratios of 0.25-0.31, 0.02 increment. McNamara et al. (1997) reported sub-Moho P-wave velocities of 7.9-8.1 km/s for the Qiangtang Terrane. We found that the sub-Moho velocity of 8.10 km/s and a mantle lid thickness of 100 km with no velocity gradient provided a good fit to the Pn waveform and arrival time (see below). Uncertainties in the Pn velocity are about 0.05 km/s based on the misfit of the Pn travel time for the paths to AMDO, WNDO and ERDO.

Figure 3a shows the observed and synthetic vertical component Pnl waveforms for station AMDO (filtered 0.01-0.1 Hz) for the crustal thickness-P-wave velocity grid and a Poisson's ratio of 0.29. Notice that decreasing the vertical P-wave travel time in the crust, either by increasing the velocity or decreasing the thickness, causes the PL waveform to arrive earlier. This effect on the Pnl waveform has been known for some time (Shaw and Orcutt, 1984; Wallace, 1986). Generally, the fits are quite good with a few models resulting in linear correlations greater than 0.9 (models indicated by grey shading). The misfit as

measured by the scaled rms-difference and linear correlation shows a minimum for station AMDO for a crustal thickness of 65 km, P-wave velocity of 6.2 km/s and Poisson's ratio of 0.29 (yielding a S-wave velocity of 3.37 km/s). Figure 3b shows the observed and synthetic radial component Pnl waveforms for station AMDO (filtered 0.01-0.05 Hz) for the same models as Figure 3a. Due to higher noise levels on the horizontal components we filtered these data in the band 0.01-0.05 Hz. Similar to Figure 3a, the trade-off between crustal thickness and velocity can be seen. For the radial component the best-fitting models are combinations of crustal thickness and P-wave velocity of: 70 km, 6.3 km/s; or 65 km, 6.2 km/s. Consideration of the vertical and radial component Pnl waveforms at stations WNDO and ERDO revealed a similar trade-off between crustal thickness and P-wave velocity with the best-fitting combination being a crustal thickness of 65 km, V_P of 6.2 km/s and Poisson's ratio of 0.29.

The best-fitting models for all combinations of crustal parameters considered all had a crustal Poisson's ratio of 0.29, which for a crustal P-wave velocity of 6.2 km/s yields a crustal S-wave velocity of 3.37 km/s. Figure 4 shows that for a fixed crustal thickness of 65 km and crustal P-wave velocity of 6.2 km/s (constant vertical crustal P-wave travel time), the best-fitting crustal Poisson's ratio is 0.29. The scaled rms-difference and linear correlation between the data and synthetic are shown. Sensitivity of the Pnl waveforms to the crustal S-wave velocity results from converted P-SV energy trapped in the crustal waveguide. The inferred crustal thickness and S-wave velocity will be verified below by considering the fit to the complete waveforms.

Complete Waveforms and Mantle Poisson's Ratio

Complete regional waveforms contain the body-waves (Pn, PL, Sn, SnSn) and the surface-waves. Sn and the surface reflected SnSn (higher mode surface waves) travel in the mantle lithosphere and are most sensitive to the sub-Moho S-wave velocities and attenuation. The surface waves are predominately sensitive to the crustal thickness and S-wave velocities and attenuation. The travel times of Pn and Sn are most strongly sensitive to the sub-Moho P- and S-wave velocities (V_P and V_S, respectively). Thus, the differential travel time between Sn and Pn provides a strong constraint on the mantle Poisson's ratio, σ. An increase in the mantle lithospheric Poisson's ratio leads to a decrease in the sub-Moho S-wave velocity (or equivalently an increase in the sub-Moho P-wave velocity) and a delay of the Sn phase relative to the Pn phase. Errors in the event location of 20 km (or errors in the origin time of 2-3 seconds) could lead to errors in the inferred uppermost mantle P-wave velocities of ± 2% as related to absolute Pn travel times. However, the relationship between differential times of Sn-Pn and mantle Poisson's ratio is insensitive to origin time errors. The P-wave and crustal parameters were held fixed to the values described above, we then computed synthetics for

sub-Moho Poisson's ratios of 0.25-0.31 with an increment of 0.01.

Figure 5 shows the vertical and radial component data and synthetics for four of the Poisson's ratios considered for the path to station AMDO. The P-wave model is identical in all cases and thus the Pn arrival times are identical. The Sn and multiple Sn arrivals come in early for mantle Poisson's ratios of 0.25 and 0.27 and late for 0.31. A Poisson's ratio value of 0.29 accurately predicts the Sn arrival on both the vertical and radial components. Uncertainty in the best-fitting Poisson's ratio is 0.01. This value for the Poisson's ratio is well determined for shallow depths in the mantle lithosphere because the body waves (Pn and Sn) sample there. Possible variations of the inferred P- and S-wave velocities with depth is more poorly constrained. Identical results for mantle Poisson's ratio were found for the paths to stations ERDO, WNDO and USHU, indicating that 0.29±0.01 is an appropriate value for the Qiangtang Terrane. The resulting sub-Moho S-wave velocity is 4.41±0.05 km/s. The vertical and radial component Pnl and Rayleigh waves are reasonably well fit by all models in Figure 5, indicating that the focal mechanism, depth and crustal velocity model, are appropriate for these paths. Notice that Figure 5 shows that the sub-Moho S-wave velocities impact the longer period Rayleigh wave on the radial component (filtered 0.01-0.05 Hz) more strongly than the Rayleigh wave on the vertical component (filtered 0.01-0.1 Hz). This is consistent with the Rayleigh wave sensitivity kernels. The radial component was filtered more strongly because the noise level was higher on this component compared to the vertical component.

Complete Waveforms and Lithospheric Structure

The lithospheric structure inferred by fitting Pnl and Sn waveforms can be checked by considering the fits to the complete waveforms, particularly the surface waves. Figure 6 shows the fit of our Qiangtang Terrane model (derived from the analysis presented above) to the three component complete waveforms for stations AMDO, WNDO, ERDO and USHU. Good fits to the three-component waveforms were obtained for the observations at AMDO and WNDO, with the body-waveforms particularly well fit. Fits to the body waves are excellent for the path to station ERDO, however, the Rayleigh waves are complex and not well fit for this path. The fit to the radial component Rayleigh wave at station USHU is not particularly good, however this path is longer and possibly more heterogeneous than those to stations AMDO and WNDO. Generally, the body-waves and the arrival time of the surface waves are well fit by our model. We found similar results when the data were filtered 0.01-0.1 Hz. It is certainly possible that the misfit of 20 second surface wave energy in the data is due to more complex layered structure in the crust or lateral heterogeneity. Future research efforts will be directed at pursuing more detailed one-dimensional structure. Clearly it is possible that misfit of the surface waveforms results from our assumption of a simple crust without a gradient.

Attenuation Structure

Our preliminary modelling efforts assumed fairly high Q values (Q_P = 675 and Q_S = 300 for both the crust and mantle lid) and focused on determining the elastic structure by fitting the arrival times of the main phases. For the long periods considered (0.01-0.05 Hz) attenuation structure did not severely impact the waveform fits. However, from consideration of frequencies of 0.1 Hz and higher attenuation is important for the paths isolated to the Qiangtang Terrane. In order to estimate attenuation, we computed synthetic seismograms for lithospheric Q_P = 50, 100, 200, 300, 400 and 500. For each model S-wave attenuation was related to P-wave attenuation by the relation: Q_P = 2.25 Q_S (e.g., Gajewski et al. 1990). Elastic structure was fixed to that described above (Table 2). Figure 7a shows the fit of the vertical component complete waveforms observed at stations AMDO and WNDO to the various Q models. The Sn, SnSn and Rayleigh waves are best-fit by Q_P = 100-200 and Q_S = 44-88, although the path to WNDO appears to prefer slightly lower Q. Higher Q_P values result in more impulsive, higher frequency energy that is not observed in the data, while Q_P of 50 results in complete annihilation of the higher frequencies. We also considered the observed and synthetic frequency spectra of the Sn and Rayleigh waves and found that Q_P = 100-200 provides a good fit to the observed spectra. Low Q values are necessary for both the crust and mantle lid in order to fit both the body and surface waves. It is important to note that although the attenuation is rather high, models with Q_P = 100-200 did not severely attenuate the high frequency Pn energy (up to 0.5 Hz). Figure 7b shows the fit of the broadband P-waveforms to the same Q models shown in Figure 7a. The P-waveform observed at station AMDO shows significant high frequency content and is well fit by Q_P = 200-300. However, the P-waveform observed at WNDO is much more severely attenuated when compared to that at AMDO. This suggests that attenuation structure could vary between these adjacent paths. The Sn and Rayleigh waves at AMDO (Figure 7a) are better fit by lower Q values (Q_P = 50-100 and Q_S = 44-88), whereas the P-waveform is best fit by Q_P = 200-300. It is possible that crustal and mantle lid attenuation are not equal or the scaling factor between Q_P and Q_S could by higher than 2.25 in order to fit the observed frequency content of P- and S-wave phases.

Mantle Lid Structure of the Qiangtang Terrane

As stated above a mantle lid thickness of 100 km with no velocity gradient was used for the investigations of crustal parameters. This was found to provide the best fit to the broadband direct P-waves for most stations. Figure 8 shows the direct P-waveforms, filtered 0.01-0.5 Hz, for stations AMDO, WNDO and ERDO along with synthetics for mantle lid thicknesses of 25, 50, 75, 100, 125 and 150 km. All other model parameters were held fixed (crustal thickness = 65 km; crustal V_P = 6.20 km/s; crustal V_S = 3.37 km/s; sub-Moho V_P =

8.10 km/s; sub-Moho V_S = 4.41 km/s). The important feature to notice is the distinct downswing between Pn and pPn at AMDO and ERDO. The models with lid thicknesses less than 75 km do not show this downswing. However, models with lid thicknesses of 75, 100 and 125 km accurately fit this downswing. Although reflectivity modelling does not allow us to decompose the earth response into its ray theoretical contributions, a possible cause of this downswing is a wide-angle reflection of a Pn wave from the top of the low velocity zone (LVZ). The top of the LVZ (bottom of the mantle lid) is represented in our models as a decrease in P-wave velocity of 0.2 km/s over a 20 km depth interval. Reflections off this boundary will have their polarity reversed relative to the incident wave. The thickness of the mantle lid affects the timing of the LVZ-reflected energy relative to the direct Pn and pPn arrivals in such a way that all three arrivals interfere to result in the synthetic waveforms seen in Figure 8. The arrival of a reflected wave from the LVZ is supported by ray tracing travel time calculations. Models without a LVZ, such as simple crust over a half-space, did not show such a strong downswing between Pn and pPn, supporting the idea that the feature results from a wide-angle reflection from the LVZ.

Whereas the waveforms shown in Figure 8 for stations AMDO and ERDO are impulsive and quite similar, the waveform at station WNDO is much broader. The waveform for station WNDO is well fit by a much thinner lid, say, 25-50 km. However, a broad waveform also could result from higher attenuation as investigated above (Figure 7b). Either the lid is much thinner on average or attenuation is stronger for the path to WNDO, or some combination of both. Note that the relative timing and amplitude of Pn and pPn are well fit for stations AMDO and ERDO. The focal depth and mechanism were investigated using various lid thicknesses. Varying the depth only impacted the relative timing of Pn and pPn, while not affecting the relative amplitudes of these broadband pulses. Clearly the energy arriving about 15 seconds after Pn in the synthetics is not present in the data. We found that the introduction of crustal layering did not affect this energy. Varying the mechanism decreased this coda energy for some mechanisms that clearly did not fit the Pn and pPn amplitudes. The differences between the best fitting lid thickness models for these adjacent paths leaves open the possibility that mantle lithospheric structure may vary greatly over scale lengths less than 100 km. Clearly modelling seismic energy down to 2 second periods for such long paths is risky as non-plane layered structure can bias results. While these results do not support a definitive statement about the thickness of the mantle lid of the Qiangtang Terrane, they suggest at the very least that the mantle lid has a minimum thickness of 25 km for the path to WNDO and 75 km for the paths to AMDO and ERDO. It is appealing to speculate that stronger attenuation results in the broad Pn pulse seen in Figures 7 and 8 at WNDO because this path traverses closest to the volcanic sites (Figure 1). If this is the case, then a mantle lid of

- 13 -

substantial thickness (75-125 km) throughout the Qiangtang Terrane with laterally varying attenuation could fit the data.

The 92/179 Events - Validation of the Qiangtang Model

Two additional events recorded by the 1991-1992 IRIS-PASSCAL deployment also provided sampling of the Qiangtang Terrane. These events occurred on the same day (June 27, 1992) in nearly the same location (Figure 1, Table 1). Because these events occurred during the dismantling of the network, only a few stations (the northern stations) recorded this event. Focal depths and mechanisms for these events were found to be identical by Zhu and Helmberger (1996b) (Table 1). The path to station WNDO provided the best pure-path sampling of the Qiangtang Terrane. Because these events are smaller (m_b = 4.6) the signal-to-noise is worse than that for the 1992/096 event, especially on the horizontal components. Figure 9 shows the fit of our Qiangtang Terrane model to the Pnl and complete vertical component waveforms for both events recorded at WNDO. The fit to the main features of these waveforms (e.g., Pnl, Sn-Pn time, Rayleigh wave) confirms that our model (QT) accurately represents the average lithospheric structure of Qiangtang Terrane.

Comparison with Previous Results

The lithospheric structure we present can be compared with previous results for the Qiangtang Terrane. Unfortunately many of the studies published prior to the 1991-2 IRIS-PASSCAL experiment suffered from a lack of resolution when compared to more recent studies. For example, many of the paths studied were not isolated to a single tectonic unit and/or the waveforms used were recorded outside the high elevations of the Tibetan Plateau (usually at distances greater than 2000 km). Most of these studies relied wholly or partly on band-limited analog data. These data were used to infer lithospheric structure by either modelling body-wave triplications (e.g., Lyon-Caen, 1986; Zhao et al., 1991) or by modelling surface wave dispersion (e.g., Chen and Molnar, 1981; Romanowicz, 1982; Chun and McEvilly, 1986; Brandon and Romanowicz, 1986; Bourjot and Romanowicz, 1992). The Pn tomography results of Zhao and Xie (1993) and McNamara et al. (1997) serve as examples of the improved resolution of Tibetan Plateau structure after the IRIS-PASSCAL experiment. Lateral variations of Pn velocity of scale length 5° were resolvable by McNamara et al. (1997), whereas the earlier work of Zhao and Xie (1993) could resolve features on scales of 6°-10°. Our study would not be possible without the use of the broadband, high dynamic range IRIS-PASSCAL data, which provided regional paths isolated to the Qiangtang Terrane.

Analysis of regional Pn arrivals recorded by the IRIS-PASSCAL experiment found evidence for a 4% Pn velocity variation and a 12 km crustal thickness variation between the

regions north and south of 32° N latitude (McNamara et al., 1995). The Pn velocity variations were clearly defined by later tomographic analysis (McNamara et al., 1997). McNamara et al. (1995) found no such north-south lateral variation in Pg velocities and concluded that crustal P-wave velocities of 6.4±0.2 km/s may be appropriate for the entire plateau, although uncertainties in event locations, especially for small events may inhibit accurate estimation of the Pg velocities. Differences in the observed intercept time of Pn arrivals for data isolated to the northern and southern plateau (3.1 seconds) can be well modelled by our crustal thickness and crustal P-wave velocity estimates (our estimate is 3.3 seconds). The Pn velocity we report for the northern Tibetan Plateau is within the values reported by McNamara et al. (1997).

The average crustal velocities we report here are slightly slower than the crustal profiles of Zhu et al. (1993) and Zhao et al. (1996). However, the crustal properties for station WNDO reported by Owens and Zandt (1996) agree excellently with our results. The vertically propagating teleseismic data used in these studies are most strongly sensitive to the crustal thickness and S-wave velocity contrasts of discontinuities in the crust, but are less sensitive to absolute velocities. The horizontally propagating waves studied here have great sensitivity to absolute velocities and crustal thickness, but less sensitivity to layered crustal structure. A certain advantage of complete waveform modelling is the ability to estimate the crustal thickness, P-wave velocity and Poisson's ratio with Pnl and then verify the S-wave velocity structure with the fits to the Rayleigh and Love waves.

It is difficult to attribute the S-wave velocities reported in early surface wave studies to a specific tectonic unit (e.g., Lhasa, Qiangtang or Songpan-Ganzi). Two exceptions are the velocity profiles reported for the Qiangtang Terrane by Brandon and Romanowicz (1986; crustal thickness 50-60 km, average crustal $V_S = 3.45$ km/s, sub-Moho $V_S = 4.4$-4.5 km/s) and Bourjot and Romanowicz (1992; crustal thickness 65 km, average crustal $V_S = 3.36$ km/s, sub-Moho $V_S = 4.6$ km/s). The mantle model of the former and the crustal model of the later agree excellently with our results. These studies used data recorded outside of the high elevations of the Tibetan Plateau, although the study by Brandon and Romanowicz (1986) used a two-event method to isolate structure with the Qiangtang Terrane. Perhaps surface wave dispersion measurements made on regional data recorded by the IRIS-PASSCAL experiment can resolve more detailed crustal S-wave velocity structure.

Our result of 4.41±0.05 km/s for the sub-Moho S-wave velocity is on the low side of the value reported by Lyon-Caen (1986). Discrepancy in these values probably arises due to different sampling of the mostly vertically propagating triplicated SS body-waves used by Lyon-Caen and the regional complete waveforms we considered. Lyon-Caen's model for the north-central Tibetan Plateau is slower on average for the upper 200 km of the mantle than

their model for the Indian Shield. This is due to a thick low velocity layer (4.40 km/s) between 115 and 175 km. It is possible that our velocity model could fit the SS triplications modelled by Lyon-Caen (1986). The higher sub-Moho S-wave velocities reported by Lyon-Caen (1986; V_S = 4.70 between 70 and 115 km) would not fit the regional waveform data we considered here. However the uppermost mantle shear velocities reported by Lyon-Caen (1986) for the Indian Shield and Lhasa Terrane (4.65-4.7 km/s) are consistent with our results (Table 2). The model proposed by Zhao et al. (1991) for the entire Tibetan Plateau is much faster than our results for the Qiangtang Terrane, however their data primarily sampled the southern and central Tibetan Plateau.

Discussion

The modelling of regional seismic waveforms presented in this paper constrains the structure of the Qiangtang Terrane lithosphere. The main results are: 1) crustal P- and S-wave velocities are 6.1-6.3 and 3.35-3.43 km/s, respectively, yielding a Poisson's ratio of 0.28-0.30; 2) the mantle lithosphere P- and S-wave velocities are 8.05-8.15 and 4.35-4.45 km/s, respectively, yielding a Poisson's ratio of 0.28-0.30; and 3) lithospheric Q is low (attenuation is high) Q_P = 100-200 and Q_S = 44-88. There is suggestive evidence that the mantle lithosphere is 75-125 km thick. However, the results for station WNDO suggest some variability in lid thickness and/or attenuation.

Results for the crust of the northern Tibetan Plateau are anomalous when compared to typical continental crust. An average crustal P-wave velocity and Poisson's ratio was recently reported to be 6.45±0.23 km/s (Christensen and Mooney, 1995) and 0.265 (Christensen, 1996), respectively. Recent studies have also reported variations of average crustal P-wave velocity and Poisson's ratio with tectonic character. Zandt and Ammon (1995) found that average values for P-wave velocities and Poisson's ratio for Mesozoic-Cenozoic orogens are 6.25 km/s and 0.25, respectively. Rodgers and Schwartz (1997) reported an average crustal P- and S-wave velocities of 6.0 and 3.46 km/s, respectively, and a Poisson's ratio of 0.25, for the Lhasa Terrane, southern Tibetan Plateau. The current results reveal a much higher crustal Poisson's ratio for the Qiangtang Terrane relative to the Lhasa Terrane. This results from 4% higher crustal P-wave velocities and 2% lower crustal S-wave velocities between the Lhasa and Qiangtang Terranes. Such low average crustal S-wave velocities in the Qiangtang Terrane, a high Poisson's ratio, low Q and the presence of volcanism in the northern Tibetan Plateau strongly suggest the presence of partial melt in the crust. Volcanism and partial melt in the crust probably result from the relatively high temperatures and partial melt in the mantle lithosphere migrating to the surface (Turner et al., 1993, 1996; McNamara et al., 1995, 1997).

The Pn velocity we report for the northern Tibetan Plateau (8.05-8.15 km/s) is near the global average Pn velocity is 8.09±0.20 km/s (Christensen and Mooney, 1995). However, the effect of overburden pressure due to a 65 km thick crust raises the uppermost mantle velocity by about 0.17 km/s. Thus, the sub-Moho P-wave velocity in the northern Tibetan Plateau would be 7.93 km/s, if the crustal thickness there was equal to the global average (39 km). The result we report for the sub-Moho Poisson's ratio is higher than that for typical mantle compositions. To demonstrate this we compared the mantle P- and S-wave velocities and Poisson's ratio for the Qiangtang and Lhasa Terranes with laboratory results for dry compositions. Results for the Lhasa Terrane (Table 2) were taken from Rodgers and Schwartz (1996, 1997). Figure 10 shows the variation of P- and S-wave velocities and Poisson's ratio versus temperature for eclogite and ultramafic mantle compositions. Physical properties of these compositions were taken from Rudnick and Fountain (1995). The temperature and pressure derivatives used for these calculations were: $\partial V_P/\partial T$ = -0.4 km/s/1000°C; $\partial V_S/\partial T$ = -0.2 km/s/1000°C; $\partial V_P/\partial P$ = +0.2 km/s/GPa; $\partial V_S/\partial P$ = +0.03 km/s/GPa; and we considered the mantle lithosphere at a depth of 80 km (pressure of 2.3 GPa). Temperature for the Qiangtang and Lhasa Terranes were taken to be 1005°C and 700°C, respectively, with uncertainties of 130°C. (McNamara et al., 1997; Ruppel and McNamara, 1997). Also indicated in Figure 10 is the dry peridotite solidus (1250°C). Near this temperature the assumption of linear temperature and pressure dependence rapidly breaks down.

Although the V_P, V_S and σ values for eclogite in Figure 10 fall within the error estimates of our Qiangtang Terrane observations, a more plausible explanation involves an ultramafic composition with some amount of partial melt. The presence of volcanism of mantle origin in the northern Tibetan Plateau (Turner et al., 1993, 1996) and the low Q values require partial melt (Sato et al., 1989). An additional constraint on mantle lithospheric composition comes from the large shear-wave splitting observed in the northern Tibetan Plateau (McNamara et al., 1994). Ultramafic compositions, containing olivine, are more strongly anisotropic and 4-5% less dense than eclogite (Rudnick and Fountain, 1995). A mantle lithosphere composed of eclogite would not likely match the observed splitting. The higher density of eclogite would lead to lead to Bouguer gravity anomaly between the southern and northern Tibetan Plateau. No such anomaly is observed (Jin et al., 1994). Thus, we prefer a mantle composed of ultramafic material with partial melt.

Figure 11 shows how the mantle Poisson's ratio is impacted by partial melt (taken from theoretical modelling of Schmeling, 1985). Various combinations of melt fraction (percent melted volume) and melt texture (spheres versus films) are shown. Depending on the melt texture, 1-10% partial melt can increase Poisson's ratio to the observed value of 0.29. However, melt fractions of more than a few percent are probably unlikely because melt can easily

be transported away from regions of high stress, such as contractional orogens. Therefore, a 1-2% melt fraction with a melt texture containing greater than about 25% films would fit the observed Poisson's ratio.

The extremely low crustal and mantle Q and the presence of partial melt we report is consistent with the absence of high-frequency Sn and Lg for the paths considered (McNamara et al., 1995, 1996) and the absence of earthquakes in the crust below 20 km depth in the Qiangtang Terrane (Zhao and Helmberger, 1991). Gajewski et al. (1990) suggested that weak Sn energy from refraction surveys could result from a depth increasing Poisson's ratio. Owens et al. (1995) investigated the effects of attenuation and negative S-wave velocity gradients in the mantle lid on high-frequency regional Pn and Sn waveforms from the 1991-2 IRIS-PASSCAL experiment. They concluded that a depth increasing Poisson's ratio, caused by a negative S-wave velocity gradient in the mantle lid, is more effective at extinguishing high frequency Sn than simple attenuation models. The longer-period data considered here does not allow us to investigate such effects because the high frequency Sn energy is clearly absent for long path lengths. Detailed structure of the uppermost mantle lithosphere may be better determined by considering shorter paths with sufficient high frequency energy. Nonetheless, a depth increasing Poisson's ratio is also consistent with the presence of partial melt in the mantle lithosphere.

A partially melted mantle lithosphere of substantial thickness in the northern Tibetan Plateau provides important constraints on models of Tibetan Plateau evolution. Turner et al. (1993, 1996) presented a model of lithospheric thickening and subsequent thinning consistent with the timing of the observed volcanism. In their model a potassium-rich layer lies within in a homogeneously thickened cold mantle lithosphere. Thinning occurs as heat conducts into the thickened mantle lithosphere and the potassium-rich layer is exposed to melting temperatures initiating the observed volcanism. The observations we present in this paper are consistent with the presence of a mantle lithosphere, with partial melt in at least the shallow mantle, that would result from lithospheric thinning as described by Turner et al. (1993, 1996). A thick mantle lithosphere (100 km) composed of ultramafic material is also appealing as it helps to explain the large shear-wave splitting observed in the northern Tibetan Plateau (McNamara et al., 1994). A thinner mantle lithosphere would require a very high degree of anisotropy to match the observed splitting. McNamara et al. (1994) proposed shear-heating as a mechanism for high temperatures and high stresses in the shallow mantle beneath the northern Tibetan Plateau. It is not possible to discriminate between different mechanisms for mantle lithospheric heating (e.g. delamination, convective erosion or shear heating). But our results can certainly rule out wholesale delamination and convective erosion of the entire mantle lithosphere beneath the northern Tibetan Plateau as these models would result in the

complete absence of a mantle lithosphere. The low S-wave velocities we report do not require asthenospheric material directly beneath the Moho, as suggested by Brandon and Romanowicz (1986) or the high lateral temperature differences of 500° proposed by Molnar et al., (1993). However, it should be noted that a mantle lithosphere containing some partial melt would be rheologically weaker than normal continental mantle and this defies the definition of the lithosphere as the rheologically strong outer layer decoupled from mantle convective motions. It is possible that the processes occurring to deform the lower lithosphere of the Tibetan Plateau cause the material there to behave in a manner that is intermediate between strong "normal" mantle lithosphere and weak partially molten asthenosphere. The exotic seismic structures we report defy conventional wisdom of average continental properties. However, the Tibetan Plateau is far and away the most anomalous continental feature on the earth's surface and thus the exotic structures we report should be considered with an open mind.

Finally, it is important to consider that Tethyan oceanic subduction was occurring beneath the Lhasa Terrane before the Indo-Eurasia collision initiated. Underthrusting of the Indian Shield mantle lithosphere to at least the northern Lhasa Terrane is a possible interpretation of the high seismic velocities observed in the southern Tibetan Plateau (e.g. McNamara et al., 1997; Rodgers and Schwartz, 1997). This suggests the possibility that rheologically weak back-arc mantle that formerly underlaid the Lhasa Terrane has been displaced northward and/or eastward and possibly thickened by the advancing Indian mantle. It is likely that this back-arc mantle was hydrated and at near solidus temperatures. The fate of this former back-arc mantle material could have played an important role in the thermal evolution of the northern Tibetan Plateau. In particular this mantle material could provide the heat and water source for thinning the mantle lithosphere and initiating the potassic melting that lead to volcanism.

Acknowledgements

Correspondence: Arthur Rodgers, Lawrence Livermore National Laboratory, L-206, P.O. Box 808, Livermore, CA 94551 USA e-mail: rodgers@s34.es.llnl.gov; phone: (510) 423-5018; fax: (510) 422-3118.

References

Allegre, C.and 34 others, Structure and evolution of the Himalaya-Tibet orogenic belt, *Nature*, *307*, 17-22, 1984.

Barazangi, M. and Ni, J., Velocities and propagation characteristics of Pn and Sn beneath the Himalayan Arc and Tibetan Plateau: possible evidence for underthrusting of Indian continental lithosphere beneath Tibet, *Geology*, *10*, 179-185, 1982.

Beghoul, N., Barazangi, M. and Isacks, B., Lithospheric structure of Tibet and Western North America: mechanisms of uplift and a comparative study, *J. Geophys. Res.*, *98*, 1997-2016, 1993.

Bird, P., Initiation of intracontinental subduction in the Himalaya, *J. Geophys. Res.*, *83*, 4975-4987, 1978.

Bourjot, L. and Romanowicz, B., Crust and upper mantle tomography in Tibet using surface waves, *Geophy. Res. Lett.*, *19*, 881-884, 1992.

Brandon, C. and Romanowicz, B., A "no-lid" zone in the central Chang-Thang platform of Tibet: Evidence from pure path phase velocity measurements of long period Rayleigh waves, *J. Geophys. Res.*, *91*, 6547-6564, 1986.

Chen, W.-P. and Molnar, P., Constraints on the seismic wave velocity structure beneath the Tibetan Plateau and their tectonic implications, *J. Geophys. Res.*, *86*, 5937-5962, 1981.

Christensen, N., Poisson's ratio and crustal seismology, *J. Geophys. Res.*, *101*, 3139-3156, 1996.

Christensen, N. and Mooney, W., Seismic velocity structure and composition of the continental crust: A global view, *J. Geophys. Res.*, *100*, 9761-9788, 1995.

Chun, K. and McEvilly, T., Crustal structure in Tibet: high seismic velocity in the lower crust, *J. Geophys. Res.*, *91*, 10,405-10,411, 1986.

Dewey, J., Shackleton, R., Chengfa, C. and Yiyin, S., Tectonic evolution of the Tibetan Plateau, *Philos. Trans. R. Soc. of London, Ser. A*, *327*, 379-413, 1988.

Dziewonski, A. and Woodhouse, J., An experiment in systematic study of global seismicity: centroid-moment tensor solutions for 201 moderate to large earthquakes of 1981, *J.*

Geophys. Res., *88*, 3247-3271, 1983.

Fielding, E., Isacks, B., Barazangi, M. and Duncan, C., How flat is Tibet? *Geology*, 22, 162-167, 1994.

Fuchs, K. and Muller, G., Computation of synthetic seismograms with the reflectivity method and comparison with observations, *Geophys. J. Royal Astro. Soc.* *23*, 417-433, 1971.

Herquel, G., Wittlinger, G., and Guilbert, J., Anisotropy and crustal thickness of Northern-Tibet. New constraints for tectonic modelling, *Geophys. Res. Lett.*, *22*, 1925-1928, 1995.

Hirn, A. and 11 others, Crustal structure and variability of the Himalayan border of Tibet, *Nature*, *307*, 23-25, 1984.

Gajewski, D., Stangl, R., Fuchs, K. and Sandmeier, K., A new constraint on the composition of the topmost continental mantle- anomalously different depth increases of P and S velocity, *Geophys. J. Int*, *103*, 497-507 , 1990.

Jin, Y., McNutt, M. and Zhu, Y., Evidence from gravity and topography data for folding of Tibet, *Nature*, *371*, 669-674, 1994.

Jobert, N., Journet, B., Jobert, G., Hirn, A. and Zhong, S., Deep structure of southern Tibet inferred from the dispersion of Rayleigh waves through a long-period seismic network; *Nature*, *313*, 386-388, 1985.

McNamara, D., Owens, T., Silver, P. and Wu, F., Shear wave anisotropy beneath the Tibetan Plateau, *J. Geophys. Res.*, *99*, 13,655-13,665, 1994.

McNamara, D., Owens, T. and Walter, W., Observations of regional phase propagation across the Tibetan Plateau, *J. Geophys. Res.*, *100*, 22,215-22,229, 1995.

McNamara, D., Owens, T., and Walter, W., Propagation characteristics of Lg across the Tibetan Plateau, *Bull. Seism. Soc. Amer.*, *86*, 457-469, 1996.

McNamara, D., Walter, W., Owens, T. and Ammon, C., Upper mantle structure beneath the Tibetan Plateau from Pn travel time tomography, *J. Geophys. Res.*, *102*, 493-505, 1997.

Molnar, P., A review of geophysical constraints on the deep structure of the Tibetan Plateau, the Himalaya and the Karakoram, and their tectonic interpretation, *Philos. Trans. R. Soc. of London, Ser. A*, *326*, 33-88, 1988.

Molnar, P., England, P., and Martinod, J., Mantle dynamics, uplift of the Tibetan Plateau, and the Indian Monsoon, *Rev. Geophys. 31*, 357-396, 1993.

Ni, J. and Barazangi, M., High-frequency seismic wave propagation beneath the Indian Shield, Himalayan Arc, Tibetan Plateau and surrounding regions: high uppermost mantle velocities and efficient Sn propagation beneath Tibet, *Geophys. J. R. Astro. Soc.*, *72*, 665-689, 1983.

Owens, T., Randall, G., Wu, F. and Zeng, R., PASSCAL instrument performance during the Tibet Plateau passive seismic experiment, *Bull. Seism. Soc. Amer.*, *83*, 1959-1970, 1993.

Owens, T., Crotwell, H. P., McNamara, D., and Randall, G., Regional wave propagation in and around the Tibetan Plateau, in Proceedings of the 17th Annual Seismic Research Symposium on Monitoring a Comprehensive Test Ban Treaty, 281-290, 1995.

Owens, T. and Zandt, G., Implications of crustal property variations for models of Tibetan Plateau evolution, *Nature*, *387*, 37-43, 1997.

Patton, H., Crustal and upper mantle structure of the Eurasian continent from the phase velocity of and Q of surface waves, *Rev. Geophys.*, *18*, 605-625, 1980.

Powell, C., and Conaghan, P., Plate tectonics and the Himalayas, *Earth Planet. Sci. Lett.*, *20*, 1-12, 1973.

Randall, G., Ammon, C. and Owens, T., Moment tensor estimation using regional seismograms from a Tibetan Plateau portable network deployment, *Geophys. Res. Lett.*, *22*, 1,665-1,668, 1995.

Romanowicz, B., Constraints on the structure of the Tibetan Plateau from pure path phase velocities of Love and Rayleigh waves, *J. Geophys. Res.*, *87*, 6,865-6,883, 1982.

Rodgers, A. and Schwartz, S., Lithospheric structure throughout Tibet from regional waveform modelling: underthrusting of the Indian Shield, felsic thickening and partial melt, (abstract) *Trans. Amer. Geophys. U. (EOS)*, *77*, F675, 1996.

Rodgers, A. and Schwartz, S., Low crustal velocities and mantle lithospheric variations in southern Tibet from regional Pnl waveforms, *Geophys. Res. Lett.*, *24*, 9-12, 1997.

Rudnick, R., and Fountain, D., Nature and composition of the continental crust: a lower crustal perspective, *Rev. Geophys.*, *33*, 267-309, 1995.

Sapin, M., Wang, X., Hirn, A. and Xu, Z., A seismic sounding in the crust of the Lhasa block, Tibet, *Annales Geophysicae*, *3*, 637-646, 1985.

Sato, H., Sacks, S., Murase, T., Muncill, G. and Fukuyama, H., Qp-melting temperature relation in peridotite at high pressure and temperature: Attenuation mechanism and implications for the mechanical properties of the upper mantle, *J. Geophys. Res.*, *94*, 10,647-10,661, 1989.

Schmeling, H., Numerical models on the influence of partial melt on elastic, anelastic and electric properties of rocks. Part 1: elasticity and anelasticity, *Phys. Earth and Planet. Inter.*, *41*, 34-57, 1985.

Searle,, M., and 10 others, The closing of Tethys and the tectonics of the Himalaya, *Geol. Soc. Amer. Bull.*, *98*, 678-701, 1987.

Shaw, P. and Orcutt, J., Propagation of PL and implications for the structure of Tibet, *J. Geophys. Res.*, *89*, 3,135-3,152, 1984.

Turner, S., Hawksworth, J., Rogers, N., Kelley, S. and van Calsteren, P., Timing of the Tibetan uplift constrained by analysis of volcanic rocks, *Nature*, *364*, 50-54, 1993.

Turner, S., Arnaud, N. Liu, J., Rogers, N., Harris, N., Kelley, S., van Clasteren, P., and Deng, W., Post-collisional, shoshonitic volcanism on the Tibetan Plateau: implications for convective thinning of the lithosphere and the source of ocean island basalts, *J. of Petrology*, *37*, 45-71, 1996.

Wallace, T., Inversion of long-period regional body waves for crustal structure, *Geophys. Res. Lett.*, *13*, 749-752, 1986.

Wittlinger, G. and 10 others, Seismic tomography of northern Tibet and Kunlun: evidence for crustal blocks and mantle velocity contrasts, *Earth Planet. Sci. Lett.*, *139*, 263-279, 1996.

Zandt, G. and Ammon, C., Continental crust composition constrained by measurements of crustal Poisson's ratio, *Nature*, *374*, 152-154, 1995.

Zhao, L. and Helmberger, D., Geophysical implications from relocations of Tibetan earthquakes: hot lithosphere, *Geophys. Res. Lett.*, *18*, 2205-2208, 1991.

Zhao, L., Helmberger, D. and Harkrider, D., Shear-velocity structure of the crustal and upper mantle beneath the Tibetan Plateau and southeastern China, *Geophys. J. Int.*, *105*, 713-730, 1991.

Zhao, L., and Xie, J., Lateral variations in compressional velocities beneath the Tibetan Plateau from Pn traveltime tomography, *Geophys. J. Int.*, *115*, 1070-1084, 1993.

Zhao, L., Sen, M., Stoffa, P. and Frolich, C., Application of very fast simulated annealing to the determination of the crustal structure beneath Tibet, *Geophys. J. Int.*, *125*, 355-370, 1996.

Zhao, W., and Morgan, J., Injection of Indian crust into Tibetan lower crust: a two-dimensional finite element model study, *Tectonics*, *6*, 489-504, 1987.

Zhou, R., Grand, S., Tajima, F. and Ding, X., High velocity zone beneath the southern Tibetan Plateau from P-wave differential travel-time data, *Geophys. Res. Lett.*, *23*, 25-28, 1996.

Zhu, L., Zeng, R., Wu, F., Owens, T. and Randall, G., Preliminary study of crust-upper mantle structure of the Tibetan Plateau by using broadband teleseismic body waveforms, *Acta Seismol. Sinica*, *6*, 305-316, 1993.

Zhu, L., Owens, T. and Randall, G., Lateral variation in crustal structure of the northern Tibetan Plateau inferred from teleseismic receiver functions, *Bull. Seismo. Soc. Amer.*,

85, 1531-1540, 1995.

Zhu, L. and Helmberger, D., Intermediate depth earthquakes beneath the India-Tibet collision zone, *Geophys. Res. Lett.*, *23*, 435-438, 1996a.

Zhu, L. and Helmberger, D., Lithospheric structure under the Tibetan Plateau from broadband seismic waveforms, *Trans. Amer. Geophys. U. (EOS)*, *77*, F691, 1996b.

Table 1. Source parameters for the earthquakes considered in this study. The depths were adjusted to fit the P and pP waveforms.

Event	Origin time (UT)	lat/lon/depth (km)	m_b	strike / dip / rake
1992/096	April 5, 1992 07:47:47.3	35.70° / 80.71° / 10	5.6	62° / 90° / -11 [#]
1992/179	June 27, 1992 02:13:18.3	35.15° / 81.08° / 5	4.6	40° / 40° / -80° [*]
1992/179	June 27, 1992 13:20:20.9	35.13° / 81.13° / 5	4.6	40° / 40° / -80° [*]

[#] mechanism adjusted from the Harvard CMT solution, dip only.

[*] mechanism provided by L. Zhu (Zhu and Helmberger, 1996b).

Table 2. Average seismic velocity model for the Qiangtang Terrane (top) and Lhasa Terrane (bottom), depth in km; velocities in km/s; gradients in s^{-1}.

depth (top)	depth (bottom)	V_P	V_S	σ	V_P gradient	Q_P
Qiangtang 0.0	4.0	5.00	2.89	0.25	0.0	200
Terrane 4.0	65.0	6.20	3.37	0.29	0.0	200
65.0	165.0	8.10	4.41	0.29	0.0	200
Lhasa 0.0	4.0	5.00	2.89	0.25	0.0	?
Terrane 4.0	70.0	6.00	3.46	0.25	0.0	?
70.0	190.0	8.25	4.63	0.27	0.002	?

Figure Captions

Figure 1. Major tectonic/geologic terranes, faults and sutures of the Tibetan Plateau and the surrounding region (faults and sutures, black lines; 3000 m elevation contour, grey lines), event, station and path locations. The focal mechanisms for the 92/096 and 92/179 events (Table 1) are also shown. Sampling locations of volcanic rocks by Turner, et al. (1993) are shown as diamonds.

Figure 2. Observed (solid) and synthetic (dashed) broadband (filtered 0.01-0.5 Hz) P and pP waveforms for different focal parameters. (a) Regional P-waveforms at six stations at different azimuths for three focal mechanisms (see text) with the depth fixed at 10 km. (b) Regional P-waveforms at station AMDO for four different depths with the focal mechanism fixed to our parameters. (c) Teleseismic vertical component P-waveforms (solid) and WKBJ synthetics (dashed) for three IRIS-GSN stations. These data were filtered 0.02-0.2 Hz.

Figure 3. Observed (solid) and synthetic (dashed) Pnl waveforms for event 1992/096 station AMDO: (a) vertical component filtered 0.01-0.1 Hz, (b) radial component filtered 0.01-0.05 Hz. Synthetics for models with various crustal thickness and P-wave velocity are shown while the crustal Poisson's ratio is fixed at 0.29. Measures of model performance are shown adjacent to each pair: scaled rms-difference, q; linear correlation, r; and Pn travel time residual, t. Models with linear correlations above 0.9 are grey shaded and the best-fitting model is outlined.

Figure 4. Observed (solid) and synthetic (dashed) vertical component waveforms for station AMDO for four values of crustal Poisson's ratio. For each model crustal thickness and P-wave velocity were fixed at 65 km and 6.2 km/s, respectively. To evaluate the fits the scaled rms-difference, q, and the linear correlation, r, between the data and synthetic are shown.

Figure 5. Observed (solid) and synthetic (dashed) complete waveforms for the station AMDO. The models for each synthetic are identical except for the sub-Moho Poisson's ratio (Pr) and S-wave velocity (Vs), indicated in the figure. Vertical components (left) and radial components (right) were filtered from 0.01-0.1 Hz and 0.01-0.05 Hz, respectively.

Figure 6. Observed (solid) and synthetic (dashed) three-component complete waveforms for stations AMDO, WNDO, ERDO and USHU. Synthetics were generated using the Qiangtang Terrane model (Table 2). Data and synthetics were filtered 0.01-0.05 Hz.
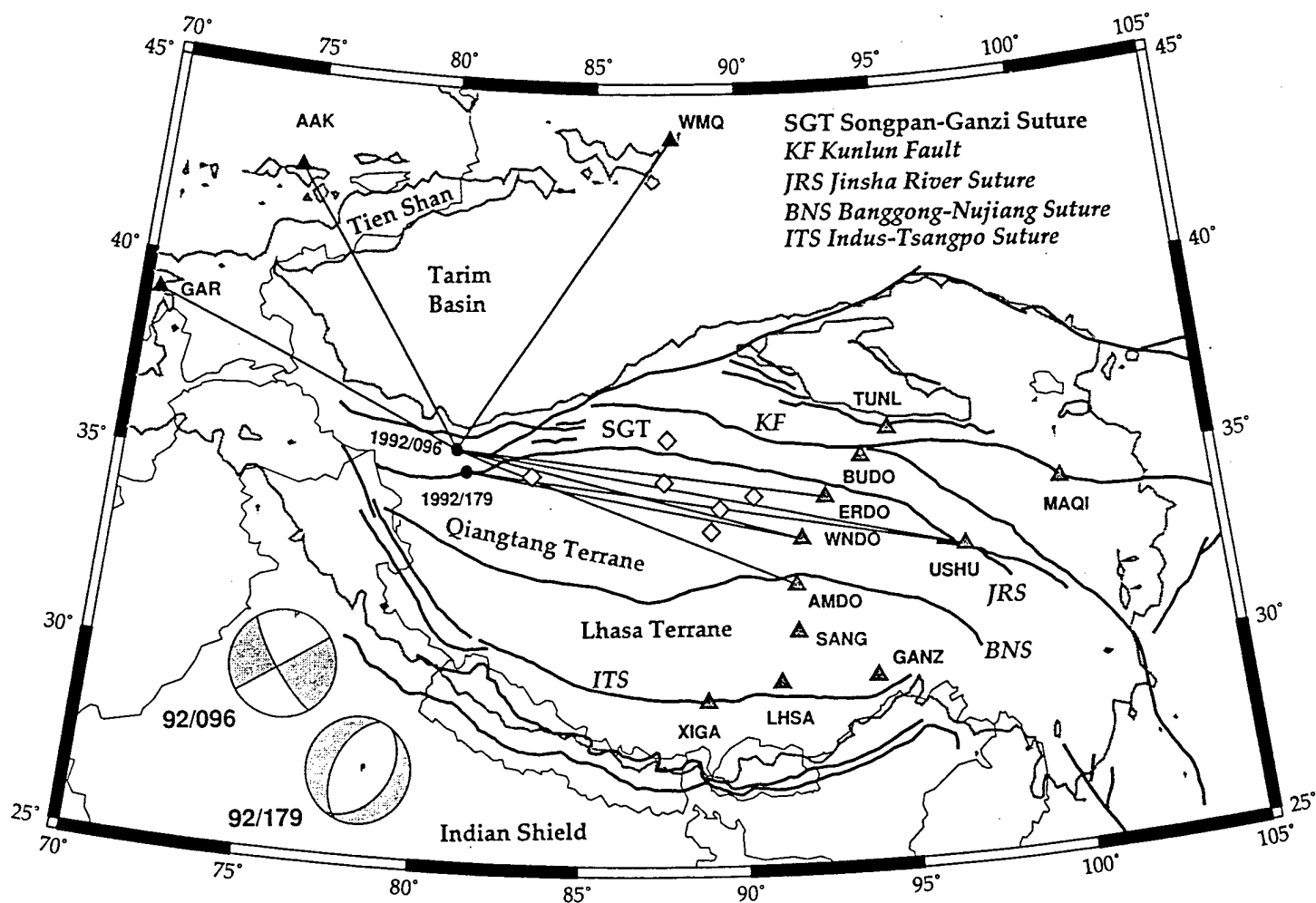
Figure 7. (a) Vertical component complete waveforms for stations AMDO and WNDO and synthetics for $Q_P = 50, 100, 200$ and 300. Elastic structure was held fixed to the QT model. The data and synthetic were filtered in the pass band 0.01-0.1 Hz. (b) Vertical component P-waveforms (filtered 0.01-0.5 Hz) for the same models as (a).

Figure 8. Observed (solid) and synthetic (dashed) vertical component waveforms for stations AMDO, WNDO and ERDO for various mantle lid thicknesses. Data and synthetic are pass band filtered 0.01-0.5 Hz. The direct phase, Pn, depth phase, pPn, and the possible low-velocity zone reflection, Plvz, are shown (ERDO 100 km lid thickness).

Figure 9. Observed (solid) and model QT synthetic (dashed) waveforms for the 1991/179 events observed at station WNDO. Vertical component complete (left, filtered 0.01-0.05 Hz) and Pnl (right, filtered 0.01-0.1 Hz) are shown.
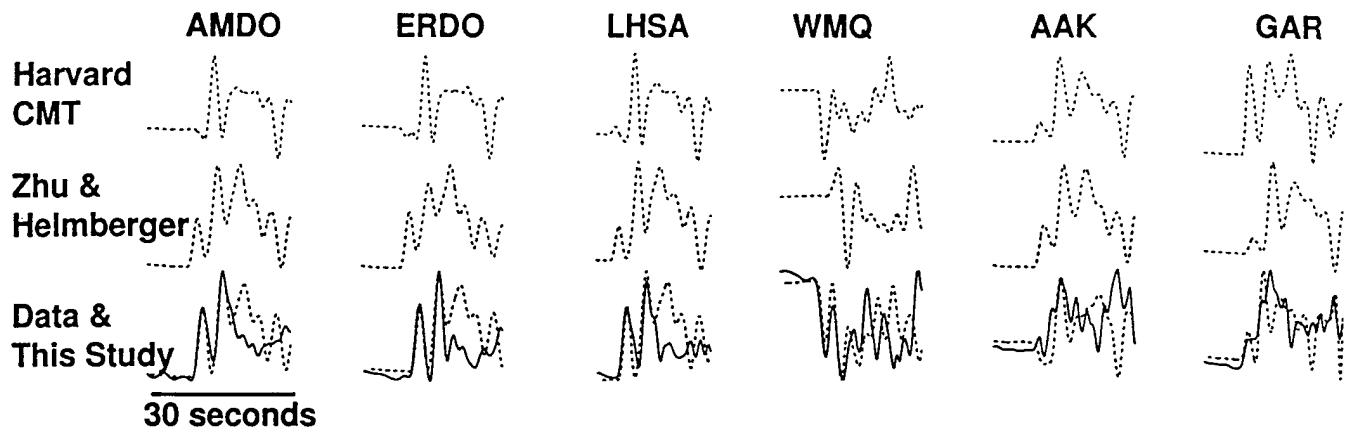
Figure 10. Comparison of observed and laboratory derived Poisson's ratio, P- and S-wave velocities. Physical properties of the eclogite and ultramafic compositions were derived from values reported in Rudnick and Fountain (1996). Temperature estimates were taken from McNamara et al. (1997).

Figure 11. Poisson's ratio versus melt fraction and texture for partially melted lithospheric mantle. Also shown is our estimate for the mantle Poisson's ratio for the Qiangtang Terrane.
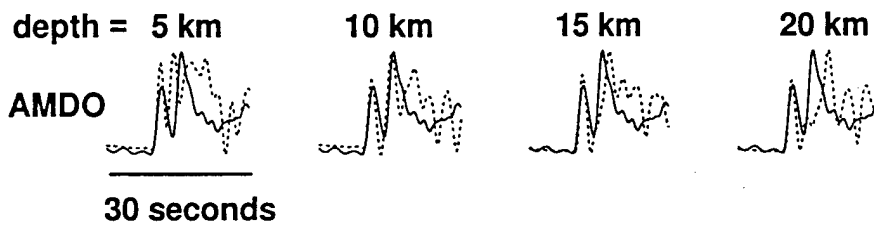
SGT Songpan-Ganzi Suture
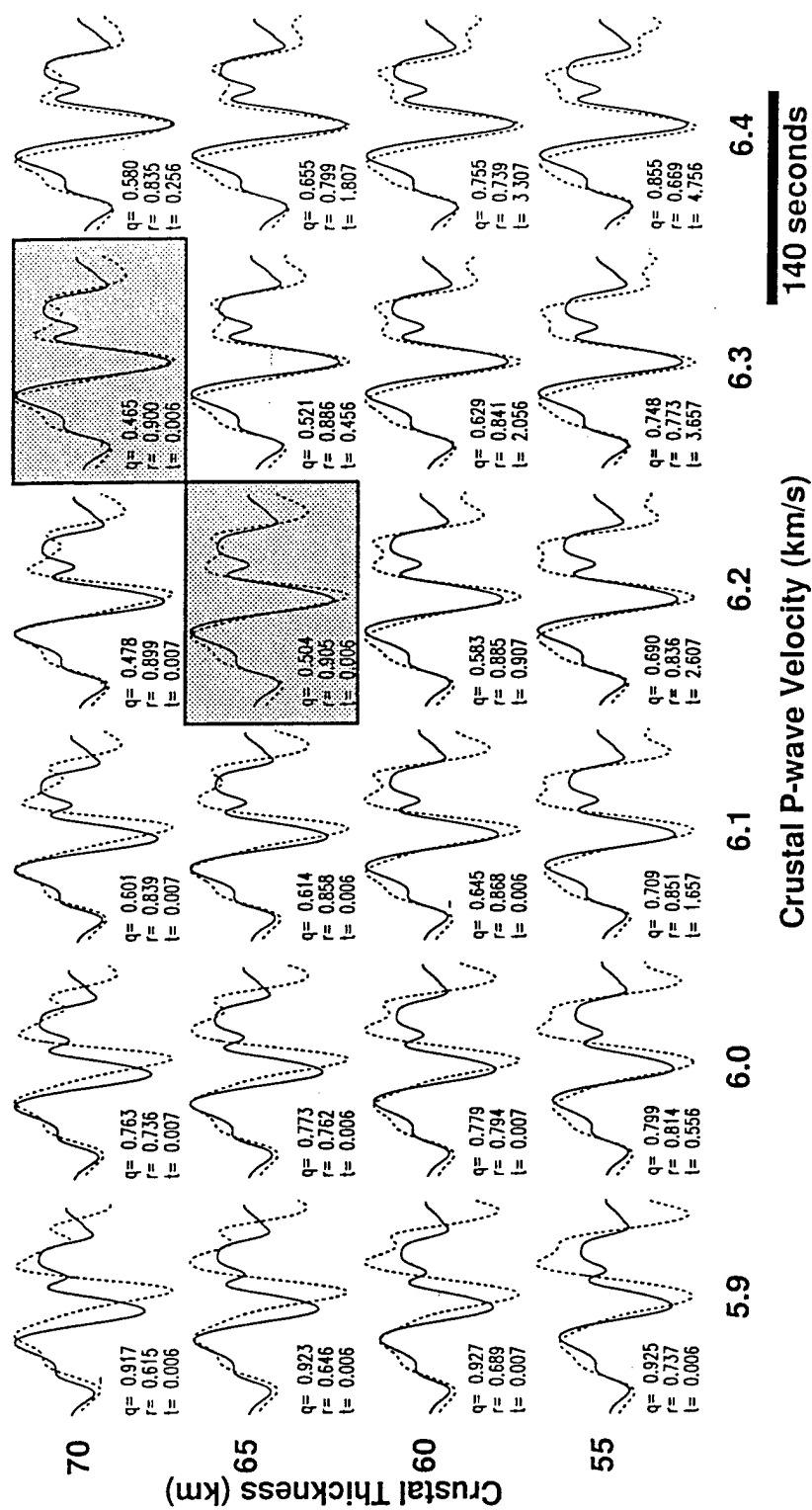KF Kunlun Fault
JRS Jinsha River Suture
BNS Banggong-Nujiang Suture
ITS Indus-Tsangpo Suture

Rodgers and Schwartz, TIBET JGR, 1997 Figure

a

AMDO   ERDO   LHSA   WMQ   AAK   GAR

Harvard
CMT

Zhu &
Helmberger

Data &
This Study

30 seconds

b

depth = 5 km   10 km   15 km   20 km

AMDO

30 seconds

c

KIV   KONO   MDJ

Harvard
CMT

Zhu &
Helmberger

This Study

50 seconds

Rodgers and Schwartz, TIBET JGR, 1997 Figure 2

Crustal P-wave Velocity (km/s)

Crustal Thickness (km)

Rodgers and Schwartz, TIBET JGR, 1997 Figure 3a

Crustal P-wave Velocity (km/s)

Crustal Thickness (km)

Rodgers and Schwartz, TIBET JGR, 1997 Figure 3b

Crustal S-wave Velocity (km/s) →

| 3.58 | 3.48 | 3.37 | 3.25 |

q= 0.744
r= 0.722

q= 0.445
r= 0.900

q= 0.335
r= 0.949

q= 0.557
r= 0.878

Crustal Poisson's Ratio →

| 0.25 | 0.27 | 0.29 | 0.31 |

120 seconds

Rodgers and Schwartz, TIBET JGR, 1997, Figure 4

Vertical, filtered 0.01-0.1 Hz

Radial, filtered 0.01-0.05 Hz

Vs = 4.25
Pr = 0.31

SnSn

Sn

Rayleigh

Pnl

Sn

Rayleigh

Pnl

Vs = 4.41
Pr = 0.29

Vs = 4.55
Pr = 0.27

Vs = 4.68
Pr = 0.25

420 seconds

Rodgers and Schwartz, TIBET JGR, Figure 5

Rodgers and Schwartz, TIBET JGR, 1997 Figure 6

a

WNDO

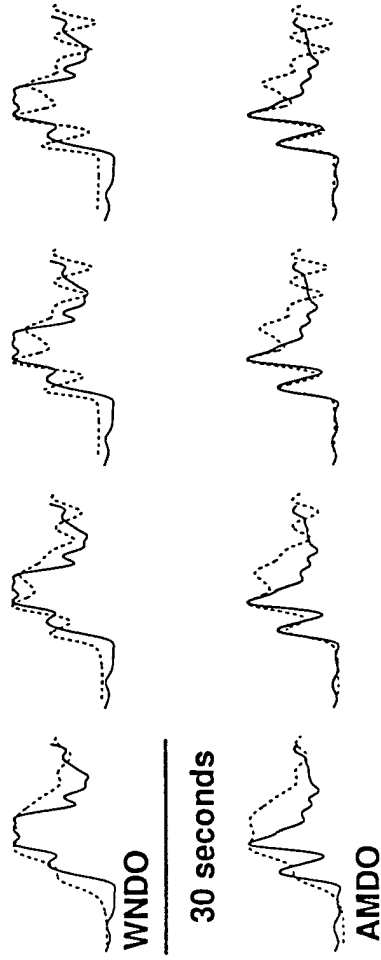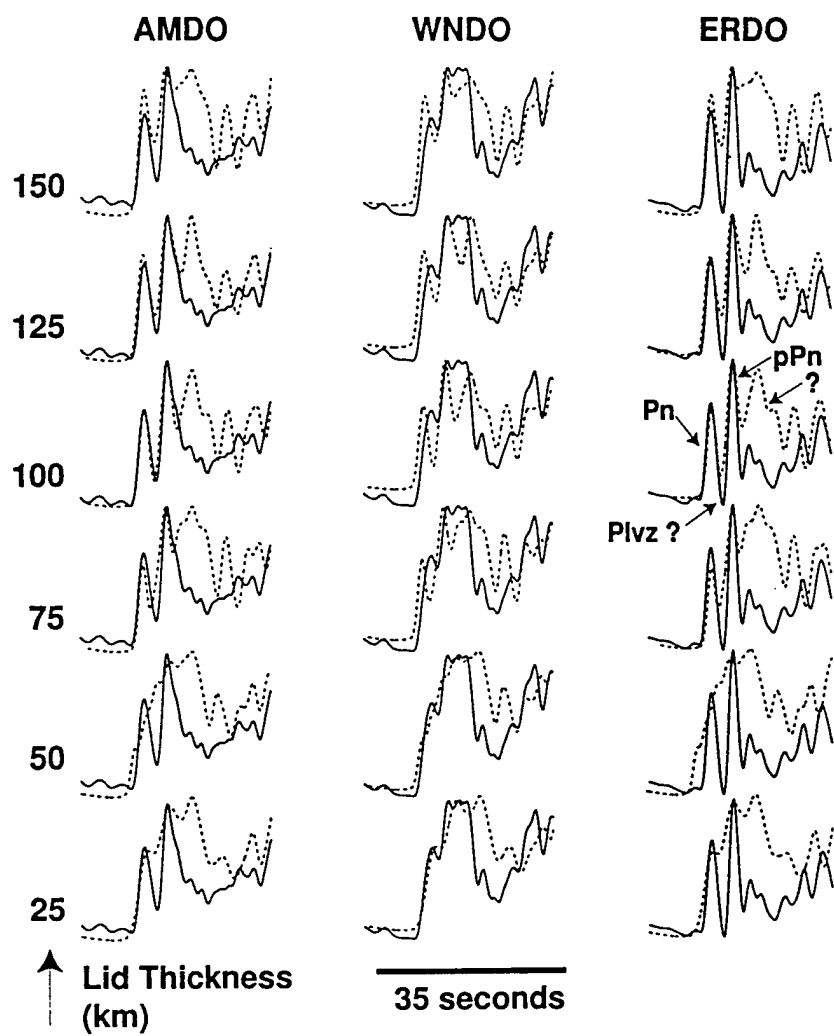370 seconds

AMDO

Qp=50
Qs=22

Qp=100
Qs=44

Qp=200
Qs=89

Qp=300
Qs=132

b

WNDO

30 seconds

AMDO

Rodgers and Schwartz, TIBET JGR, 1997 Figure 7

AMDO   WNDO   ERDO

150

125

100

75

50

25

↑ Lid Thickness
   (km)

35 seconds

pPn
?
Pn
Plvz ?

Rodgers and Schwartz, TIBET JGR, 1997 Figure 8

Complete Waveforms

Pnl Waveforms

Pnl   Sn   Rayleigh

WNDO

92/179/13:20:20

WNDO

92/179/02:13:18

330 seconds

120 seconds

Rodgers and Schwartz, TIBET JGR, 1997, Figure 9

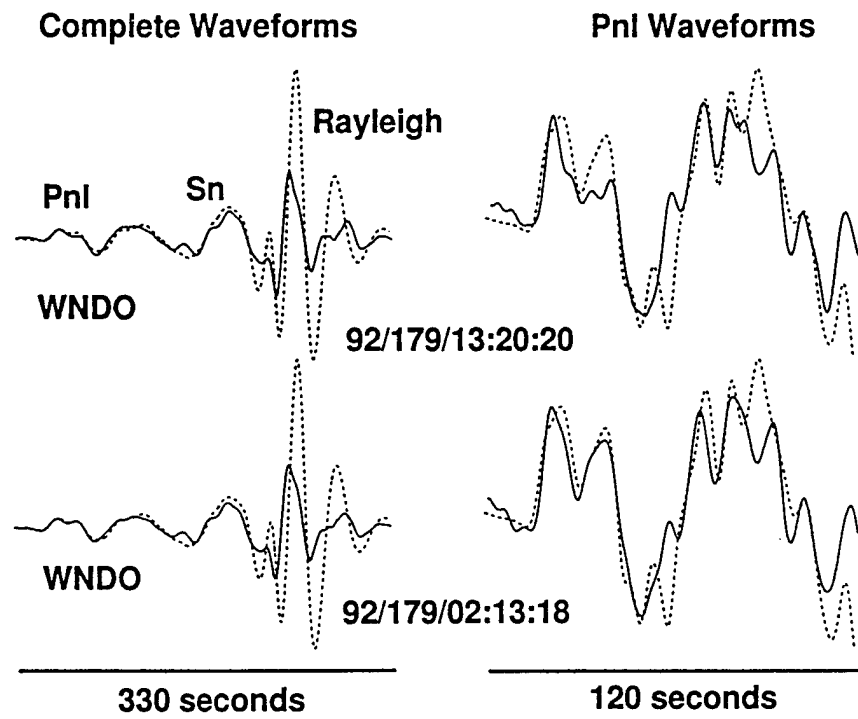Rodgers and Schwartz, TIBET JGR, 1997, Figure 10

Poisson's Ratio vs. Melt Fraction and Texture

Rodgers and Schwartz, TIBET JGR, 1997, Figure 11